Cement and Concrete Research 151 (2022) 106636

Contents lists available at ScienceDirect

Cement and Concrete Research

journal homepage: www.elsevier.com/locate/cemconres

Effect of alkali hydroxide on calcium silicate hydrate (C-S-H)

Yiru Yan [a,b,*], Sheng-Yu Yang [c], George D. Miron [d], Ines E. Collings [e], Emilie L'Hôpital [a], Jørgen Skibsted [c], Frank Winnefeld [a], Karen Scrivener [b], Barbara Lothenbach [a,f,g]

[a] Empa, Swiss Federal Laboratories for Materials Science and Technology, Laboratory for Concrete & Asphalt, Überlandstrasse 129, 8600 Dübendorf, Switzerland
[b] EPFL, STI IMX LMC, MXG 230, Station 12, CH-1015 Lausanne, Switzerland
[c] Department of Chemistry and Interdisciplinary Nanoscience Center, Aarhus University, Langelandsgade 140, DK-8000 Aarhus C, Denmark
[d] Paul Scherrer Institute, Laboratory for Waste Management, Forschungsstrasse 111, 5232 Villigen PSI, Switzerland
[e] Center for X-ray Analytics, Swiss Federal Laboratories for Materials Science and Technology, Überlandstrasse 129, 8600 Dübendorf, Switzerland
[f] University of Bern, Institute of Geological Sciences, Rock-Water Interaction Group, Hochschulstrasse 6, 3102 Bern, Switzerland
[g] NTNU, Department of Structural Engineering, 7491 Trondheim, Norway

ARTICLE INFO

Keywords:
Cement
C-S-H
Alkali hydroxide
Ca/Si ratio
Characterization

ABSTRACT

This paper investigates the effect of KOH and NaOH on C-S-H structure and solubility. Both KOH and NaOH have a similar effect, they increase pH values and silicon concentrations, and decrease calcium concentrations. At higher alkali hydroxide concentrations, more portlandite precipitates, while amorphous silica dissolves. This increases the $Ca/Si_{C\text{-}S\text{-}H}$ at low Ca/Si_{target} but lowers the maximum $Ca/Si_{C\text{-}S\text{-}H}$ from 1.5 to 1.2 in 1 M KOH/NaOH. The amount of alkalis bound in C-S-H increases with increasing alkali hydroxide concentrations and is higher at low $Ca/Si_{C\text{-}S\text{-}H}$. KOH/NaOH lead to a structural rearrangement in C-S-H, increasing the interlayer distance, number of layers stacked in *c* direction and shortening the silica chains. The mean chain lengths (MCL) estimated from FTIR and Raman spectroscopy agree well with the trends from ^{29}Si NMR. Comparison with the independently developed CASH+ thermodynamic model showed a good agreement between the observed and modelled changes, including the shortening of the MCL.

1. Introduction

Cement, with an annual consumption of 4 billion tons, is the most used construction material [1]. The main cement hydration product is calcium-silicate-hydrates (C-S-H), which makes the major contribution to the strength and other properties of hydrated Portland cement [2–4]. The structure and properties of C-S-H, as the most important component in hydrated cement, has been investigated in a large number of studies, see e.g. [5–10] and references cited therein. As shown in Fig. 1, C-S-H has a layered structure, with calcium oxide layers sandwiched between silicate chains in a "dreierketten" arrangement. Within the silicate chains, the two "pairing" silicate tetrahedra coordinate with Ca in the calcium layer, while the third silicate tetrahedron, the bridging Si site, links two pairs of silicate units. The silicate chain length is influenced by the Ca/Si ratio as demonstrated in several ^{29}Si NMR studies [5,11–18] over the last decades. Bridging silicate tetrahedra are mainly present in C-S-H with low Ca/Si and largely absent at high Ca/Si. Between the layers of Ca—O sheets and silicate chains, an interlayer region is present, which contains water molecules, Ca^{2+}, and possible alkali ions (Na^+ and/or K^+).

The alkali concentration in cement-based materials varies strongly depending on the cement composition. In the pore solution of blended cements and low alkali cements, ≈ 0.1 M alkali concentrations can be observed, while in most Portland cements alkali concentrations are between 0.3 and 0.5 M, and up to 1 M and even above in alkali-activated cementitious materials [20,21]. The alkali hydroxide concentrations in the pore solution can affect the durability of concrete as the hydroxide concentration has a significant effect on the conductivity of the pore solution as well as on the development of the alkali silicate reaction (ASR) in concrete [22,23].

The alkali hydroxide concentration in solution determines the pH value and thus indirectly also the Ca and Si concentrations. A higher pH value will lower the dissolved Ca concentration and increase Si concentrations [24–27]. The alkali uptake in C-S-H is strongly influenced by the dissolved alkali concentration and Ca/Si of C-S-H. The alkali species are incorporated into the interlayer and on the surface via a charge

* Corresponding author at: Empa, Swiss Federal Laboratories for Materials Science and Technology, Laboratory for Concrete & Asphalt, Überlandstrasse 129, 8600, Dübendorf, Switzerland
E-mail address: yiru.yan@empa.ch (Y. Yan).

https://doi.org/10.1016/j.cemconres.2021.106636
Received 8 June 2021; Received in revised form 3 October 2021; Accepted 4 October 2021
Available online 19 October 2021

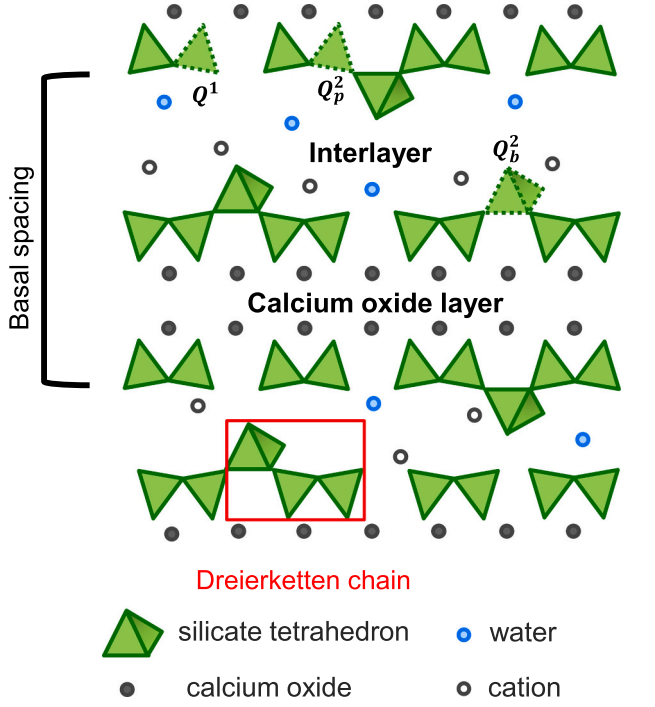

Fig. 1. Schematic structure of C-S-H. Grey circles: calcium ion; empty circles: cations in the interlayer, blue circles: water molecules in the interlayer; tetrahedra: SiO_4^-, Q^n: n indicates the numbers of Si tetrahedral neighbors, b: bridging position, p: pairing position. Adapted from [19]. (For interpretation of the references to colour in this figure legend, the reader is referred to the web version of this article.)

balance mechanism [24,26–29]. The silicate chains are negatively charged, depending on pH, which can be compensated by cations, i.e. Ca^{2+}, H_3O^+ and Na^+ or K^+ [30]. The higher the pH value, the higher is the negative charge [28,31–33]. Bivalent cations such as calcium are strongly preferred compared to monovalent sodium or potassium due to stronger electrostatic interaction [28,33]. Thus less alkalis are taken up at higher Ca/Si, as the alkali ions compete with calcium ions to compensate the negative surface charge of C-S-H. The maximum Na/Si and K/Si reported in the literature are in the range of 0.3–0.7 at $Ca/Si_{C\text{-}S\text{-}H} < 1.0$ [26,27,34,35]. Different approaches are reported in the literature to model thermodynamically the equilibrium between C-S-H and solution as discussed in detail in [5], although only few models are able to describe the incorporation of alkalis in C-S-H. High alkali concentrations result in a shorter mean silica chain length and larger interlayer distances [26,27]. In addition, the uptake of alkalis in the interlayer and the surface shifts the ^{29}Si NMR resonances to less negative values [26,27,36].

However, the interplay between alkali hydroxides in solution, the structure of C-S-H and alkali binding by C-S-H is still not fully understood, as most studies focus either on the study of aqueous concentrations [37] or on the characterization of the solid phases [36]. Moreover, there are important discrepancies among the results reported, some research observed a preference of K compared to Na uptake in synthetic C-S-H [24,38–40], while some found a higher sorption of Na than K in hydrated Portland cement [41], and other studies showed no significant difference between Na and K uptake in synthetic C-S-H [26,27,34,37,42]. The discrepancies indicate either that a large experimental error is associated with the alkali uptake measurements and/or different mechanisms are responsible for the alkali uptake in C-S-H depending on Ca/Si, equilibration time or the experimental procedure.

FTIR and Raman have been applied on C-S-H measurement in several papers [43–46], but the bands assignments of C-S-H are contradictory because of the overlapping of spectral bands, resonance splitting and different factors distorting translational symmetry of real crystals (solid solutions involving different complex anions, alterations of different kinds of stacking of layer, local defects. etc.) [47]. Based on detailed comparison of NMR, FTIR and Raman spectra we aim to use FTIR and Raman as tools to quantify the silica species in C-A-S-H and the mean chain length.

The present study also aims to explain the interplay between aqueous concentrations and C-S-H composition and the influence of KOH and NaOH, and more specifically to study the C-S-H structure by a range of spectroscopic methods and powder X-ray diffraction as well as by comparison to a newly developed thermodynamic model for C-S-H with alkali, the CASH+ model [48,49], which has been developed independently. The results and comparisons presented are particularly pertinent for the further development of this and other thermodynamic models to predict of pH values and alkali concentration in hydrating Portland cements and blended cements.

2. Methods

2.1. Synthesis

C-S-H was synthesized by mixing stoichiometric amounts of SiO_2 (Aerosil 200, Evonik), CaO (obtained by calcining $CaCO_3$ (Merck Millipore) at 1000 °C for 12 h), and NaOH/KOH solutions with concentrations of 0, 0.1, 0.5 or 1 M at a water/solid ratio of 45. The targeted molar Ca/Si ratio were $Ca/Si_{target} = 0.6$, 0.8, 1.0, 1.2, 1.4 and 1.6. The C-S-H samples were equilibrated for 3 months. The sample preparation, filtration and washing were following the procedure described in detail in L'Hôpital et al. [18]. The samples were freeze-dried for 7 days and then stored in N_2 filled desiccators in the presence of saturated $CaCl_2$ solutions (RH ≈ 30%) and NaOH as CO_2 trap [18].

2.2. Analytical methods

2.2.1. Solution analysis

The composition of the liquid phase was analysed by ion chromatography (IC) as soon as possible after filtration in solutions diluted by factor 10, 100 and 1000 with MilliQ water to avoid any carbonation or/and precipitation. The concentrations of Ca, K, Na, and Si were quantified using a Dionex DP series ICS-3000 ionic chromatography system. Independent measurements of solutions with known compositions indicated a measurement error of ≤10%.

The pH measurements were carried out with a Knick pH meter (pHMeter 766) equipped with a Knick SE100 electrode. The calibration pH electrode follows the method detailed in [50]: the electrode was calibrated against NaOH or KOH solutions of known concentrations to minimise alkali error. The pH were measured at laboratory temperature (23 to 24 °C) and corrected to 20 °C taking into account the effect of temperature on the pH measurement.

2.3. Solid phase analysis

Thermogravimetric analyses (TGA) were conducted on ground powder (~20–30 mg) under nitrogen atmosphere at a heating rate of 20 °C/min from 30 to 980 °C with a Mettler Toledo TGA/SDTA 8513 instrument. Mass losses between 30 °C and ~ 600 °C were assigned to dehydration and dehydroxylation of C-(N, K-)S-H and portlandite during heating. Portlandite was quantified based on the weight loss between ~350 and ~ 600 °C using the tangential method [51]. Quantification of portlandite by TGA instead of XRD Rietveld analysis was preferred due to the possible presence of nano-crystalline portlandite at high alkali concentrations.

Powder X-ray diffraction (XRD) data were collected using a PANalytical X'Pert Pro MPD diffractometer equipped with rotating sample stage in a θ-2θ configuration applying Cu radiation (λ = 1.54 Å) at 40 mV voltage and 40 mA, with steps of 0.019° 2θ with a fixed divergence slit

size and an anti-scattering slit on the incident beam of 0.25° and 0.5° 2θ. The samples were scanned between 5° and 70° 2θ with an X'Celerator detector. Profile fittings are conducted to calculate the *d*-spacing and the full width at half maximum (FWHM) of the (002) reflection of C-S-H. The diffraction profiles were calculated with Pseudo-*Voigt* function using the software package Highscore Plus V 3.0e. The observed reflections could all be assigned based on the Powder Diffraction File for portlandite (PDF# 00-044-1481) and tobermorite MDO2 (11 Å structure) from Merlino et al. [52] for C-S-H. In the case of C-S-H with targeted Ca/Si = 1.0 and synthesized in 1.0 M KOH, an additional impurity phase of $K_2CO_3{\cdot}1.5H_2O$ (PDF# 00-011-0655) was present.

The domain sizes, referred to as crystallite sizes, were calculated by fitting the C-S-H powder XRD patterns using Pawley refinements in Topas [53] with the starting unit cells of tobermorite 11 Å ($a = 6.732(2)$ Å, $b = 7.369(1)$ Å, $c = 22.680(4)$ Å, $\gamma = 123.18(1)°$, space group *B*11*m*) or 14 Å ($a = 6.735(2)$ Å, $b = 7.425(2)$ Å, $c = 27.987(5)$ Å, $\gamma = 123.25(1)°$, space group *B*11*b*) [52,54]. A standard sample of CaF_2 was used to account for the instrumental peak broadening. The peak profile parameters, taken from the CaF_2 refinement, were kept fixed for all the C-S-H samples. The additional anisotropic peak broadening arising from the sample as a consequence of different crystallite sizes was refined using the AnisoCS macro [55] where two peak broadening terms were refined: one along the *a*- and *b*-axes, and one along the *c*-direction. In the case of 1.0 M NaOH concentration, two tobermorite phases with different *c* lattice parameters and different domain size along the *c*-axis were refined to account for the double d_{002} reflection. All other unit cell parameters and the crystallite size along the *ab*-directions were kept identical between the two phases.

Attenuated total reflectance (ATR) Fourier Transformation-Infrared (FTIR) spectra were collected by averaging 32 scans measured on a Bruker Tensor 27 FTIR spectrometer by transmittance between 340 and 4000 cm^{-1} at a resolution of 4 cm^{-1} on ~3 mg of powder. The IR spectral data obtained were preprocessed using the software package OPUS (Bruker Optics GmbH, Ettlingen, Germany). Baseline correction and normalization to the intensity of the peak at around 950 cm^{-1} were applied to every recorded spectrum.

The Raman spectra were recorded using a Raman Bruker Senterra microscope equipped with a Peltier-cooled CCD detector and a 20 mW laser. The software Opus 6.5 was used to analyse the spectra. A lens with a magnification of 50× and a green laser with a wavelength of 532 nm were used. The integration time was 10 s and each spectrum was recorded two times at spectrum resolution of 3–5 cm^{-1}. The spectra were background corrected and normalized based on the intensity of the peak at around 670 cm^{-1}.

The ^{29}Si MAS NMR spectra were acquired on a Bruker-400 (9.39 T) spectrometer using a Bruker ^{1}H - X 4 mm MAS probe and a spinning speed of $\nu_R = 10.0$ kHz. The spectra used single-pulse excitation with a pulse length of 1.75 μs for an rf field strength of $\gamma B_1/2\pi = 71$ kHz, a recycle delay of 30 s, and 2048 scans. The ^{29}Si chemical shifts are referenced to tetramethylsilane (TMS), using an external sample of belite, β-Ca_2SiO_3, at −71.33 ppm as a secondary reference[56].

Deconvolutions were carried out with the dmfit software [57]. The peak shapes were constraint with Lorentzian/Gaussian ratio = 0.5, FWHM ≤3.0 ppm for all resonances, following the description in ref. [58]. The structure of the drieketten structure of the silica chains was respected by keeping two pairing tetrahedra (Q_p^2) for one bridging tetrahedron, $I(Q_p^2)/I(Q_b^2) = 2$ (with $I(Q_p^2) = I(Q_{pa}^2) + I(Q_{pb}^2)$). The Q_{pa}^2 resonance is located at ~ −85 ppm and the Q_{pb}^2 peak at ~ −88 ppm, and Q_{pb}^2 is only observed for C-S-H samples with Ca/Si < 1.0, which indicates the chemical environment of Q_{pa}^2 and Q_{pb}^2 is different. The Q_{pa}^2 and Q_{pb}^2 assignments are discussed in more detail in ref. [58]. The main chain length (MCL) were calculated using the equation:

$$MCL = \frac{2\left(Q^1 + Q_p^2 + Q_b^2\right)}{Q^1} \quad (1)$$

2.4. C-S-H composition

The effective Ca/Si in C-S-H ($Ca/Si_{C\text{-}S\text{-}H}$) was obtained by mass-balance calculations, considering the initial amount of CaO and SiO_2 in the system, the amount of other solids present as well as the fraction of SiO_2 and CaO in solution following the procedure outlined in [19]. The amount of bound water in C-S-H was determined by TGA based on the weight loss between 30 and ~ 600 °C minus water in portlandite.

The amount of alkalis bound in the solid was determined following the **direct method** (i.e. complete re-dissolution of 20 mg of washed and dried C-S-H phase in 10 mL 100 mM HCl). The total amount in the solid was obtained from the measured Ca, Na and K concentrations in the HCl solution as detailed in [26]. The amount of alkali was also obtained indirectly from mass balance calculations using the total amount of alkalis present minus the fraction which remained in the equilibrium solution; this **indirect method** gives comparable results to the direct method up to 0.1 M NaOH and KOH (see also [26]). At higher alkali concentrations, however, the indirect method fails as the deduction of high measured concentrations to obtain a small amount of absorbed alkali ions results in a too large errors to allow any meaningful conclusions.

2.5. Thermodynamic modelling

Thermodynamic modelling was carried out with the Gibbs free energy minimization program GEM-Selektor v3.7 [59]. GEMS is geochemical modelling code that computes equilibrium speciation of dissolved species and stable solid phases composition using Gibbs free energy minimization algorithms. The thermodynamic data for aqueous, solid, and gaseous phases were taken from the PSI-Nagra thermodynamic database [60], while the solubility products for cement minerals were taken from the Cemdata18 database [61]. C-S-H and alkali uptake was modelled using the CASH+ thermodynamic model [48,49], that was parameterized against experimental data independent of this study. The formation of the $CaSiO_2(OH)_2^0$ was described using a formation constant of log K = 4.0 for the equation $Ca^{2+} + SiO_2(OH)_2^{2-} \Longleftrightarrow CaSiO_2(OH)_2^0$ [48] instead of the log K of 4.6 from [60].

3. Results and discussion

3.1. Effect of Ca/Si on liquid and solid phase composition

The Ca/Si ratio affects greatly the composition of the equilibrium solutions in the absence of alkali hydroxides as shown in Fig. 2, where changes of Ca, Si and OH^- concentrations are plotted as a function of the Ca/Si in C-S-H. The Ca/Si in C-S-H ($Ca/Si_{C\text{-}S\text{-}H}$) varies between ≈ 0.75–1.44 for Ca/Si_{target} from 0.6 to 1.6, as at very low Ca/Si_{target} amorphous silica precipitates in addition to C-S-H and at high Ca/Si_{target} portlandite [5]. At low Ca/Si_{target}, the Si and Ca concentrations are in the mM range; the silicon concentrations decrease down to 0.004 mM at high Ca/Si_{target}, while Ca concentrations increase up to 21 mM in the presence of portlandite. The measured trends and concentrations agree well with other observations reported in the literature as summarized in e.g. the recent review of Walker et al. [6], and with the changes modelled by using the CASH+ thermodynamic model [48], although the model somewhat underestimates the Ca and overestimates the Si concentrations. At the lowest total Ca/Si_{target} of 0.6, the thermodynamic model predicts in addition to low $Ca/Si_{C\text{-}S\text{-}H}$ C-S-H the presence of a small amount of amorphous SiO_2 (16% of the total silica present in the sample).

C-S-H is the main solid phase observed for every targeted Ca/Si. In addition to C-S-H, portlandite is precipitated at $Ca/Si_{target} = 1.6$ (see Fig. 3 (a)), while amorphous SiO_2 is observed at $Ca/Si_{target} = 0.6$ resulting in effective $Ca/Si_{C\text{-}S\text{-}H}$ of 0.75 to 1.44. All aqueous concentrations, the effective C-S-H composition and the amount of minor phases

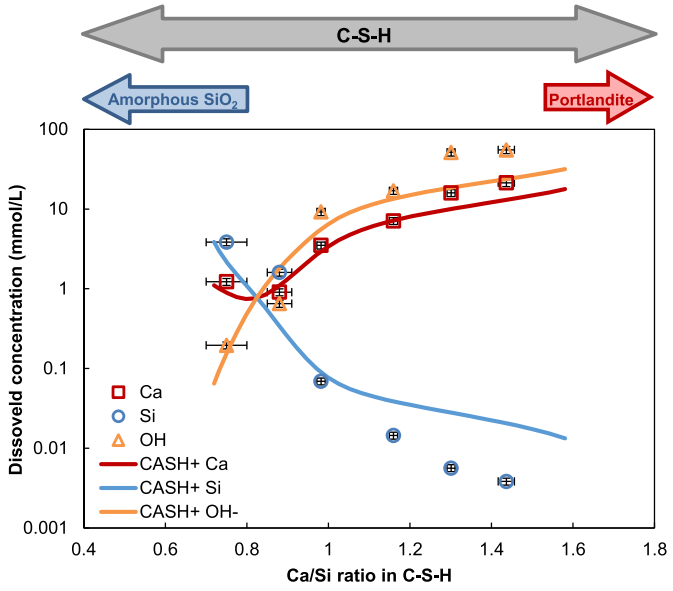

Fig. 2. Concentrations of Ca, Si and OH^- in solutions equilibrated with C-S-H samples as a function of the Ca/Si ratios in C-S-H. Yellow triangles: OH^-, red squares: Ca and blue circles: Si. Solid lines: simulated using the thermodynamic CASH+ model [48,49]. The estimated absolute errors of $Ca/Si_{C\text{-}S\text{-}H}$ are smaller than ±0.05 units in the Ca/Si ratios. The estimated relative uncertainty of the IC measurements is ±10%, which is smaller than the size of the symbols. (For interpretation of the references to colour in this figure legend, the reader is referred to the web version of this article.)

are reported in Tables A1–A3. A closer inspection of the XRD diffractograms summarized in Fig. 3 (a) shows that for high Ca C-S-H the lowest-angle diffraction peak (d_{002}), indicating the basal spacing of C-S-H, is more distinct and that the interlayer distances are getting smaller. The decrease in basal spacing could be related to the charge balancing effect of Ca^{2+} in the C-S-H interlayer, which may increase the attractive force between the negatively charged main layers [62]. The broad reflection at ~17° 2θ (d-spacing ~5 Å), which has been assigned to a d_{101} signal and indicates occupation of bridging Si-sites [63], is well visible at low $Ca/Si_{C\text{-}S\text{-}H}$, where the bridging silica are present and absent at high $Ca/Si_{C\text{-}S\text{-}H}$, where the bridging sites are empty, which has also been observed in XRD studies on C-S-H [63]. The tendency is in agreement with ^{29}Si NMR studies (e.g. [18], Fig. 3 (b)).

The NMR spectra in Fig. 3 (b) show resonances between −75 to −90 ppm, which are simulated using four resonances with chemical shifts (δ_{iso}) of ~−79 ppm (chain-end sites, Q^1), −82 ppm (bridging sites Q_b^2), −85 ppm and − 87 ppm (paired sites, Q_{pa}^2, and Q_{pb}^2) with the restriction that the intensities fulfill the condition, $[I(Q_{pa}^2) + I(Q_{pb}^2)]/I(Q_b^2) = 2$ imposed by the dreierketten model, as discussed in detail by Yang et al. [58]. In C-S-H with low $Ca/Si_{C\text{-}S\text{-}H}$, mainly Q^2 sites are present indicating the predominance of connected silicate chains and a small number of Q^1 groups from the end of the silica chain. The Q^1 intensity increases with Ca/Si such that at $Ca/Si_{C\text{-}S\text{-}H} = 1.30$ and 1.44 mainly dimers (Q^1 species) are observed, in agreement with the previous observations [11–14,16,18,27]. The decrease of Q^2 and increase of Q^1 species leads to a decrease of the mean chain length from 76 ± 15 at $Ca/Si_{C\text{-}S\text{-}H} = 0.75$ to 2.5 ± 0.1 at high $Ca/Si_{C\text{-}S\text{-}H}$ (see Table 1). The MCL values at low Ca/Si are somewhat larger than those derived earlier for similar samples, which varied from 20 to 37 [12,16–18]. This may reflect differences in equilibration time during synthesis and the fact that the precision in MCL is very sensitive to small intensity variations at low values for the Q^1 intensities (see Eq. (1)).

Fig. 3 (c and d) show the FTIR and Raman spectra of C-S-H. Since the Si—O bonds are the strongest bonds in the structure with a covalent character, different types of Si—O can be recognized in the infrared spectra; the position of transmittance bands is affected slightly by the ions in the second coordination sphere [64]. From 400 cm^{-1} to 800 cm^{-1}, the spectra have contributions from bending vibrations of the O-Si-O groups in the dreierketten chains and from water librations, while the bands in the region 800–1200 cm^{-1} are due to stretching vibration of Si—O [47,65].

In FTIR the bending vibrations at wavenumbers from 500 to 800 cm^{-1} can be considered as a "fingerprint region" sensitive to the composition and the topological features of the tetrahedral frameworks [47]. The bands observed are consistent with the FTIR spectra of C-S-H at different Ca/Si reported e.g. in Yu et al. [46]. The bands from 400 to 550 cm^{-1} are assigned to deformations of Si tetrahedra [46,65]; the intensity of the shoulder at 480 cm^{-1} increases clearly with $Ca/Si_{C\text{-}S\text{-}H}$, which indicates there is also a Q^1 signal hidden under it. The band at 670 cm^{-1} has been related to Si-O-Si (O-Si-O) bending [46,65] and water librations [65] and shows little variation upon an increase of $Ca/Si_{C\text{-}S\text{-}H}$. The signal at 810 cm^{-1} is related to Si—O stretching of Q^1 tetrahedra [46]. The strong increase of its intensity at high $Ca/Si_{C\text{-}S\text{-}H}$ agrees well with the increase of the Q^1 signal reported from Si-NMR studies [17,19] and Fig. 3 (b). At 960 cm^{-1} the main peak is observed and is associated with Si—O stretching modes [65]. An increase of the $Ca/Si_{C\text{-}S\text{-}H}$ leads to a shift to lower wavenumber (940 cm^{-1}), indicating progressive depolymerisation of the silicate chains. A shoulder on the low-frequency side of the Q^1 signal marked as * is also detected in C-S-H with $Ca/Si_{C\text{-}S\text{-}H}$ from 1.16 to 1.44, while no literature was found to give interpretation of this signal. The main peak of the FTIR spectra located between 940 and 960 cm^{-1} has often been assigned in the literature to Q^2 vibrations [44,46,66,67], however, its predominance for all $Ca/Si_{C\text{-}S\text{-}H}$ and the observed shift indicate rather that the band observed is composed of several overlying vibrations including a Q^2 signal at ≈ 960 cm^{-1} [68], which results in the observed shift to higher wavenumbers for low $Ca/Si_{C\text{-}S\text{-}H}$. A shoulder on the low-frequency side of the main peak located at ≈ 930 cm^{-1} detected in C-S-H with $Ca/Si_{C\text{-}S\text{-}H}$ from 0.67 to 0.98 is interpreted as Q_b^2 due to Si—O stretching modes within OH-SiCa configurations in the bridging tetrahedron [65]. A shoulder on the high-frequency side located at ≈1050 cm^{-1} is also detected arising at increased $Ca/Si_{C\text{-}S\text{-}H}$ and interpreted as Si—O stretching including Si—O stretching in Q_b^2 [65].

The Raman spectra in Fig. 3 (d) also provide vibrational information; the strongest vibrational modes active in Raman are those that related to the greatest polarizability; symmetric vibrational modes are most Raman active. From 150 cm^{-1} to 400 cm^{-1}, the spectra have contributions from Ca^{2+} motions in the region <250 cm^{-1} [69] and the lattice vibrations of Ca—O at 316–333 cm^{-1} [70]. The intensity of the Ca—O band increases with increasing $Ca/Si_{C\text{-}S\text{-}H}$ and shifts from 316 cm^{-1} at $Ca/Si_{C\text{-}S\text{-}H} = 0.75$ to 333 cm^{-1} at $Ca/Si_{C\text{-}S\text{-}H} = 1.44$. A small shoulder 350 cm^{-1} appears at $Ca/Si_{C\text{-}S\text{-}H} = 1.44$, which is assigned to portlandite [70,71]. A major band at 445 cm^{-1} is assigned to internal deformation of the Si-tetrahedra [69] or to O-Si-O bending [70]; its intensity increases with Ca/Si. The main Si-O-Si symmetrical bending peak at ~675–680 cm^{-1} broadens with increasing $Ca/Si_{C\text{-}S\text{-}H}$, which agrees with the study of Garbev et al. [70]. The peak has been assigned to Q^2 symmetrical bending [69,70], however, as this peak is dominant both at high and low $Ca/Si_{C\text{-}S\text{-}H}$, further vibrations not related to Q^2 species contribute to this signal. The Si—O silicate symmetrical stretching (SS) band at ~870–900 cm^{-1} is assigned to SS Q^1; its intensity increases strongly with Ca/Si and thus the fraction of Q^1 species present. The band at 950–1010 cm^{-1} has been assigned to SS Q^2 [14,69,70,72], however, as its intensity does not decrease at higher $Ca/Si_{C\text{-}S\text{-}H}$, a number of other vibrations seem to contribute. The peaks located at 1080 cm^{-1} are attributed to the C—O SS vibrations [69–71,73] and are identified in every spectrum as Raman is very sensitive to even small CO_2 contaminations.

The mean silicate chain length (MCL) calculated from FTIR and Raman as well as thermodynamic CASH+ models are compared with values from ^{29}Si NMR as illustrated in Fig. 4. The CASH+ model shows the same trends but a somewhat weaker increase of MCL at low Ca/Si,

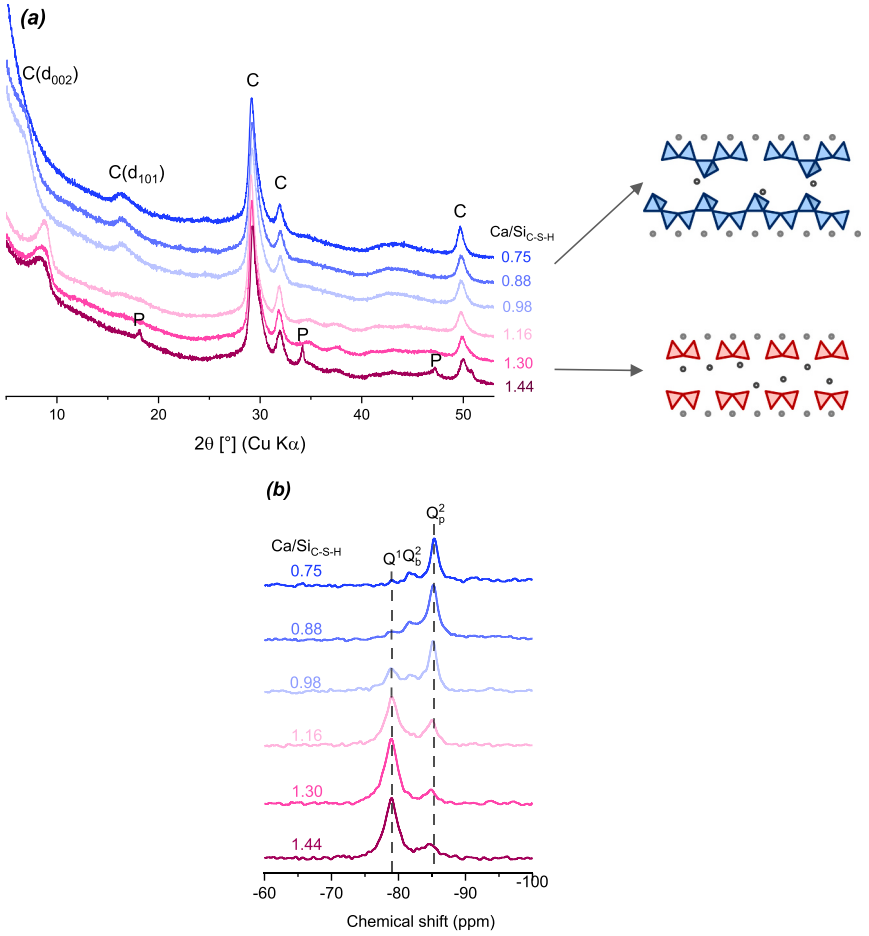

Fig. 3. (a) XRD diffractograms of the C-S-H samples synthesized in water and C-S-H schema for C-S-H with low Ca and high Ca. (b) ^{29}Si NMR spectra, (c) FTIR and (d) Raman spectra of C-S-H with $Ca/Si_{C\text{-}S\text{-}H}$ from 0.75 to 1.44, after an equilibration time of 3 months. C: C-(K-)S-H; P: portlandite.

which is related to higher MCL observed in the present study. The MCL of FTIR and Raman are calculated based on the peak area ratio of the Q^1 signal at ~810 and the main peak at ~960 cm^{-1} from FTIR, and Q^1 signal at ~880 and the main peak at 670 cm^{-1} from Raman. The MCL calculated from FTIR, Raman, and NMR decreases as the $Ca/Si_{C\text{-}S\text{-}H}$ increases, confirming agreement among the different spectroscopic methods. For C-S-H with every $Ca/Si_{C\text{-}S\text{-}H}$, FTIR overestimates the MCL because the IR spectrum in the main peak region contains very complicated series of overlapping bands. Raman shows better agreement with the NMR quantification because the peaks are more separated but for C-S-H with $Ca/Si_{C\text{-}S\text{-}H} = 0.75$, the signal to noise ratio is lower than the others, which makes the quantification error larger. For C-S-H with $Ca/Si_{C\text{-}S\text{-}H} > 1.0$, dimers dominate in C-S-H so the MCL is around 2.5. The difference of MCL from FTIR, Raman and NMR is smaller when $Ca/Si_{C\text{-}S\text{-}H}$ is above 1.15, but the calculation of Q^1 species shows a much greater difference as shown in Fig. A1, while this is not well visible in Fig. 4.

3.2. Effect of NaOH/KOH on the aqueous phase

In the absence of KOH or NaOH, the measured aqueous Ca concentrations and pH values increase with rising Ca/Si_{solid}, while the Si concentrations decrease as shown in Fig. 2. Fig. 5 illustrates that the presence of NaOH or KOH leads to higher pH values and silica concentrations, but lower Ca concentrations; no significant difference was observed between NaOH and KOH. The measured concentrations are consistent with existing solubility measurements in the $CaO\text{-}Al_2O_3\text{-}Na_2O/K_2O\text{-}SiO_2\text{-}H_2O$ systems between 20 and 25 °C [16,19,26,27,74–76], which all show comparable trends in dissolved Si, Ca and pH values with respect to the bulk alkali content and Ca/Si ratio.

In the presence of KOH and NaOH, the dissolved Si and Ca concentrations show similar trends as in their absences: a rise of Ca and a decline of Si concentrations with increasing Ca/Si (Fig. 5). This suggests that C-(N, K-)S-H solubility does not vary greatly as a function of the alkali cation (Na or K) present, but that the concentrations are just shifted to higher pH values, due to the common ion effect with C-S-H between pH, Ca and Si. The measured pH values, alkali (data in Table A1), Ca and Si concentrations can be well reproduced by thermodynamic modelling using the recent CASH+ solid solution model [48,49]. In agreement with the experimental data, no significant differences are observed in the modelled results, independent of whether NaOH or KOH are used.

The thermodynamic model predicts higher pH values in the presence of alkali hydroxides and increased Si concentrations due to the preference of Si to form negatively charged complexes such as $SiO(OH)_3^-$ and $SiO_2(OH)_2^{2-}$ at higher pH values. This tendency of silicon to remain in solution at high pH values leads to a complete dissolution of SiO_2 at 0.5 M NaOH and above and to a decrease of the calculated $Ca/Si_{C\text{-}S\text{-}H}$ from 0.75 (no alkali) to ~0.7 at 0.1, 0.5, and 1 M NaOH, due to the limited availability of SiO_2 in the experimental system studied.

In the presence of portlandite, the opposite effect can be observed: a decrease of Ca/Si in C-S-H at higher NaOH concentrations. Higher pH values and thus higher OH^- concentrations decrease the Ca concentrations in equilibrium with portlandite which lowers Ca-uptake in C-S-H.

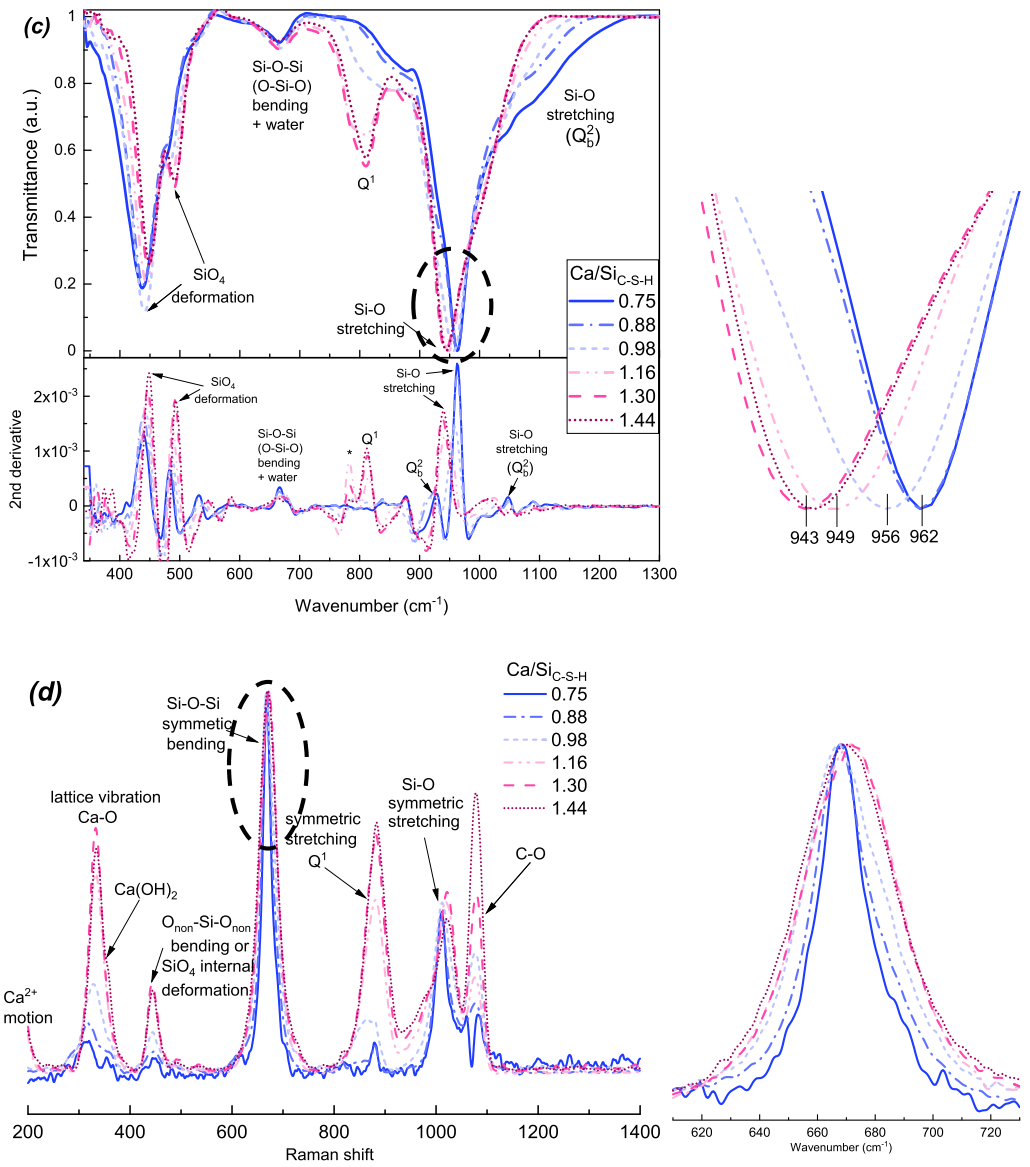

Fig. 3. (*continued*).

Table 1
Secondary phase quantification and mean silica chain length (MCL) of C-S-H samples without alkali.

Ca/Si_{target}	Ca/Si_{C-S-H}	SiO_2 amorphous (wt %)[a]	Portlandite (wt %)[b]	MCL[a]
0.6	0.75 ± 0.05	10 ± 2	0	76 ± 15
0.8	0.88 ± 0.03	4.0 ± 1.0	0	27 ± 7
1.0	0.98 ± 0.01	0	0	9.1 ± 1.3
1.2	1.16 ± 0.01	0	0	3.5 ± 0.2
1.4	1.30 ± 0.01	0	0	2.55 ± 0.10
1.6	1.44 ± 0.02	0	0.9 ± 0.1	2.56 ± 0.10

[a] Amorphous SiO_2 and MCL quantified from ^{29}Si NMR.
[b] Portlandite quantified by TGA.

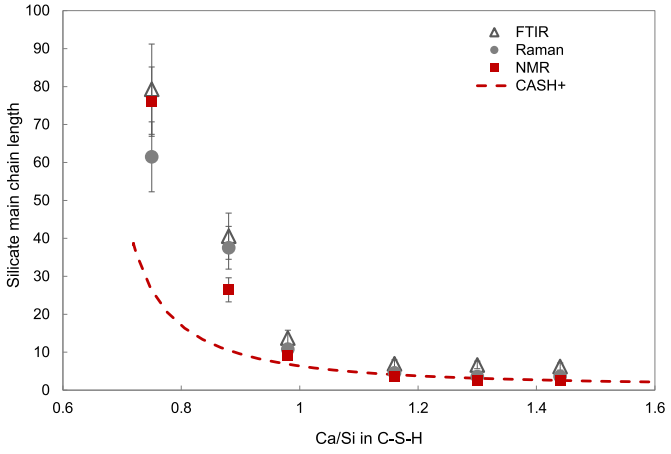

Fig. 4. Silicate main chain length determined by FTIR, Raman, ^{29}Si NMR, and thermodynamic CASH+ model.

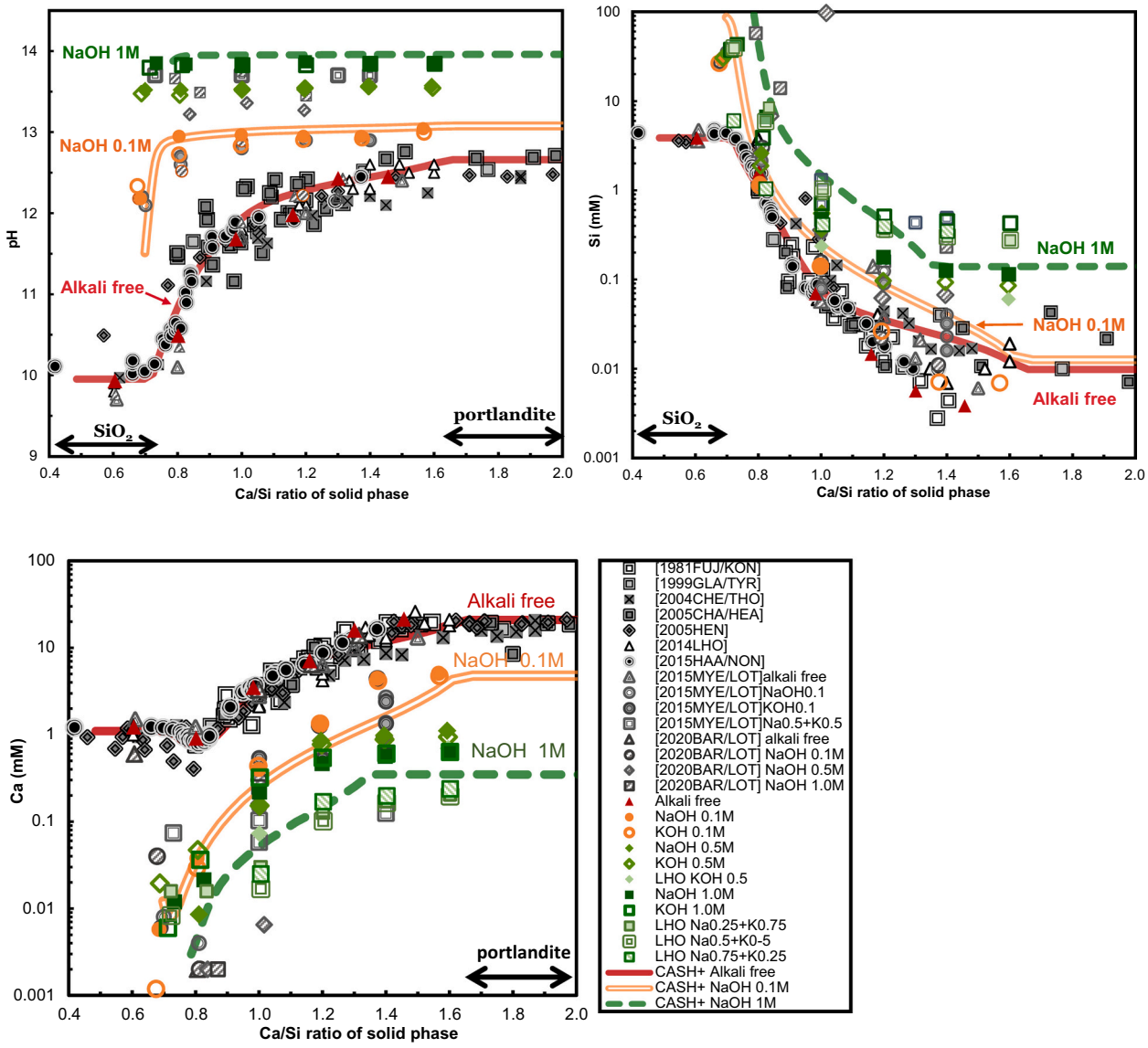

Fig. 5. pH values, Si and Ca concentrations in the solutions of the C-(N,K-)S-H samples as a function of Ca/Si ratios in C-(N,K-)S-H. The estimated absolute errors are ≤±0.05 units in the Ca/Si ratios and ± 0.2 in pH. The estimated relative uncertainty of the IC measurements is ±10%. Grey symbols: synthetic C-S-H data from [5,6,25,27]; colored symbols: C-(N,K-)S-H from this study; red triangles: C-S-H in water; orange circles: C-(N,K-)S-H with 0.1 M alkali hydroxide solution, light green diamonds: C-(N,K-)S-H with 0.5 M alkali hydroxide solution, dark green squares: C-(N,K-)S-H with 1 M alkali hydroxide solution; filled symbol: C-(N,K-)S-H with NaOH solution; empty symbol: C-(N,K-)S-H with KOH solution. Lines: simulated using the thermodynamic CASH+ model [48,49].

In the presence of portlandite, Ca concentrations decrease from 21 mM to 5 mM (0.1 NaOH), 0.8 (0.5 M NaOH) and 0.3 mM Ca in 1 M NaOH leading to a decrease of the maximum calculated $Ca/Si_{C\text{-}S\text{-}H}$ from 1.44 at 0 and 0.1 M NaOH to 1.35 at 0.5 M NaOH and to 1.07 at 1 M NaOH as detailed also in Table A2.

3.3. Effect of NaOH/KOH on C-S-H

3.3.1. Alkali uptake in C-S-H

The alkali uptake by C-S-H measured using the direct and indirect methods is plotted in Fig. 6. Determination using the indirect mass balance approach does not give meaningful results at 0.5 M alkali hydroxide and above due to large increase of the absolute error in the amount taken up at higher alkali concentrations as discussed in detail in [26]. At 0.1 M NaOH or KOH, no systematic difference was observed between the direct and indirect method.

The amount of Na and K incorporated in the C-(N,K-)S-H is higher at low $Ca/Si_{C\text{-}S\text{-}H}$ than at high $Ca/Si_{C\text{-}S\text{-}H}$ ratio. For C-(N,K-)S-H at 0.1 M alkali hydroxide, bound alkalis decreases from alkali/Si ≈ 0.20 ± 0.05 for $Ca/Si_{C\text{-}S\text{-}H} = 0.7$ to alkali/Si <0.05 for $Ca/Si_{C\text{-}S\text{-}H} = 1.35$ to 1.5. For C-(N,K-)S-H with 0.5 M alkali hydroxide, bound alkalis also decline from alkali/Si ≈ 0.6 ± 0.1 in C-(N,K-)S-H with low $Ca/Si_{C\text{-}S\text{-}H}$ to around 0.3 ± 0.1 at C-(N,K-)S-H with high $Ca/Si_{C\text{-}S\text{-}H}$. This trend and the measured alkali/Si ratios are consistent with those reported in earlier studies of alkali uptake in laboratory synthesized C-(N,K-)S-H at room temperature [24,26,34,37,77]. No significant difference between K and Na uptake was observed in agreement with the data reported by Hong and Glasser and L'Hôpital et al. [26,77]. The experimental data is satisfactorily reproduced by the model at alkali concentrations of 0.1 M and 0.5 M and for $Ca/Si_{C\text{-}S\text{-}H}$ ratios larger than 0.9. At alkali concentrations of 0.5 and low Ca/Si ratios, the model underestimates the experimental data (Fig. 6). Compared to the experimental data that shows a monotonous decrease of alkali uptake with increasing Ca/Si ratio, the CASH+ model predicts a maximum uptake around $Ca/Si_{C\text{-}S\text{-}H} = 0.77$ (0.1 M alkali), which could be a model artifact. At these conditions the model simulates that the alkalis enter the C-S-H interlayer and have little competition

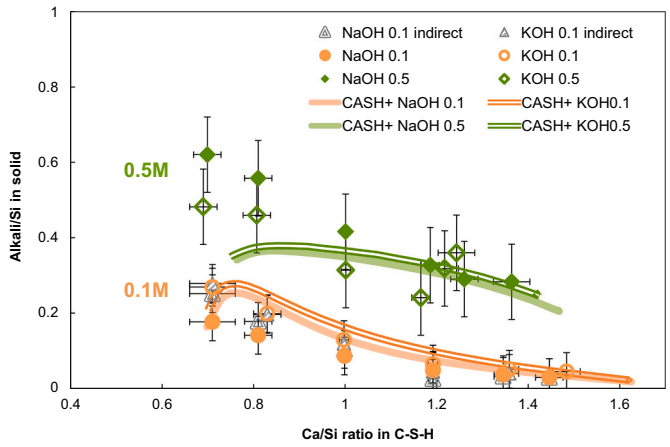

Fig. 6. Alkali uptake in C-(N,K-)S-H as a function of the Ca/Si ratio, for samples synthesized with NaOH (filled symbols) and KOH (empty symbols) equilibrated for 3 months determined by the direct method. Orange circles: C-(N,K-)S-H synthesized with 0.1 M alkali hydroxide; green diamonds: C-(N,K-)S-H synthesized with 0.5 M alkali hydroxide. Lines: simulated using the thermodynamic CASH+ model [48,49]. The estimated absolute errors were ± 0.08 units in the (Na, K)/Si ratios of the C-(N,K-)S-H products synthesized with 0.5 M alkali hydroxide and ± 0.04 units of the C-(N,K-)S-H products synthesized with 0.1 M alkali hydroxide. The estimate errors of $Ca/Si_{C\text{-}S\text{-}H}$ were smaller than ± 0.05.The values determined indirectly by mass balance at 0.1 M (grey triangles) are given for comparison. (For interpretation of the references to colour in this figure legend, the reader is referred to the web version of this article.)

from Ca. The uptake is further enhanced in the model by the presence of less Si bridging tetrahedra compared to conditions at lower Ca/Si (i.e., 0.73) and higher MCL values. Above the Ca/Si = 0.77 ratio, the decrease in alkali uptake is due to the increasing competition with Ca for the C-S-H interlayer. At high alkali concentration, e.g., 0.5 M and low Ca/Si ratio, the increase in pH results in that the model predicts that Si bridging tetrahedra are replaced by vacancies (silica becomes more soluble with increasing pH). In fact, this leads to a higher model calculated Ca/Si ratio in C-S-H (around 0.77) for conditions with the lowest target Ca/Si. The model is not compared to the experimental data carried out at 1 M alkali hydroxide due to the very large uncertainty for the experimental data at such a high concentration.

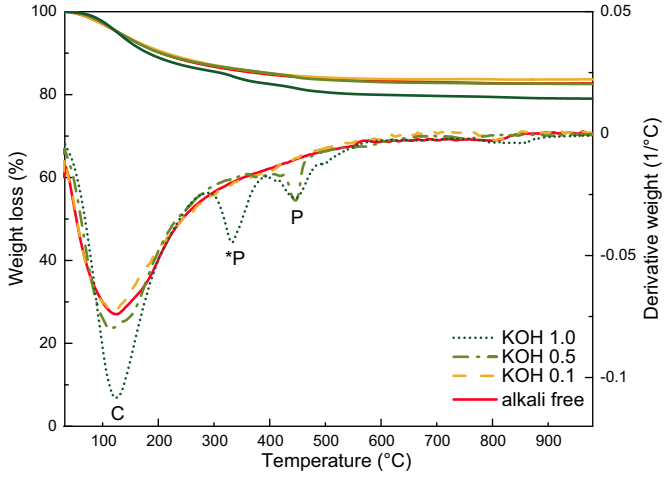

Fig. 7. TGA of C-(K-)S-H with target Ca/Si = 1.2 after an equilibration time of 3 months at different KOH concentrations. C: C-(K-)S-H; P: portlandite. *P: The weight loss between 300 and 400 °C in 1 M KOH is tentatively assigned to finely dispersed portlandite. Similar weight losses have also been observed for C-N-S-H.

3.3.2. Water content in C-S-H

Fig. 7 shows the effect of KOH concentration on TGA of C-(K-)S-H with Ca/Si_{target} of 1.2. The presence of alkali hydroxide increases moderately the amount of water present. The weight losses observed by TGA for the alkali free sample can be subdivided into a main weight loss at around 120 °C, which continues to reduce up to 600 °C associated with interlayer and surface water of C-S-H and a weaker weight loss in the range 600–980 °C, which has been assigned to the destabilization of C-S-H to wollastonite ($CaSiO_3$) and rankinite ($Ca_3Si_2O_7$) [78,79] as well as to the presence of carbonates. The TGA data confirm that in all cases C-S-H is the main solid precipitated. In 0.5 and 1 M KOH solution, in addition some portlandite is observed, in agreement with other observations on synthetic C-S-H in the presence of KOH or NaOH [19,25,26]. At 1 M KOH concentration, the TGA data indicate an additional weight loss at around 380 °C, in agreement with the observations reported for C-N/K-A-S-H in [27], which has been double checked with the XRD Rietveld quantification and is tentatively assigned to finely dispersed portlandite.

The TGA data were used to quantify the H_2O content in C-(N,K-)S-H based on the mass loss between 30 °C and 600 °C, after correction for the presence of portlandite. The H_2O/Si ratio has been measured on C-(N/K-)-S-H samples equilibrated for more than 2 weeks at ~30% RH, where mainly interlayer water plus a layer of surface water is present, but no gel water [80]. In the absence of alkalis, C-S-H products typically contain 1.2 to 1.5 H_2O per Si (Fig. 8), which agrees well with other observations of the H_2O content of C-S-H at ambient temperatures [5,15,26,27]. The H_2O/Si increases with the Ca/Si ratio, while it remains rather constant if expressed as H_2O per gram of C-S-H and decreases if expressed as H_2O/Ca as discussed in L'Hôpital et al. [18]. The presence of 0.1 M alkali hydroxide had little effect on the measured H_2O/Si, while higher alkali concentrations increased the amount of bound water, indicating that the Na^+ and K^+ present in the interlayer or surfaces of C-S-H are associated with additional water [5,15,26,27]. No significant difference could be observed between Na and K.

3.3.3. Basal spacing and crystallite size

In parallel to the water content, also the basal spacing of the dried C-S-H increases with the KOH concentration. The XRD data in Fig. 9 indicate decrease of the (002) reflection [24,52] from 8.9 to 6.9° 2θ in the presence of KOH corresponding to an increase from 9.9 Å to 12.8 Å

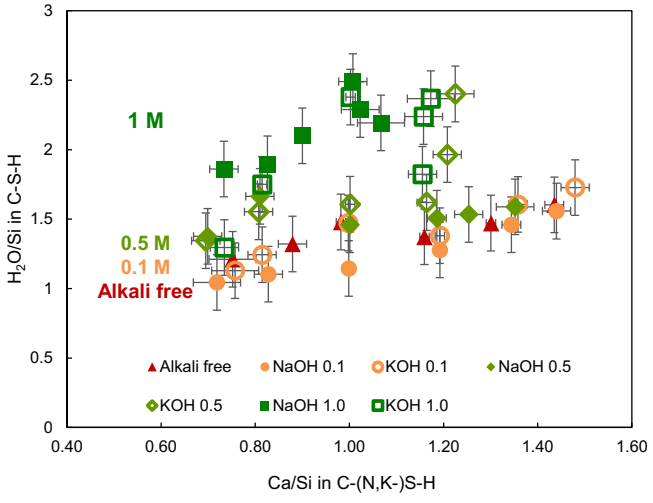

Fig. 8. H_2O/Si ratios of the C-(N,K-)S-H as functions of the Ca/Si ratio, for samples synthesized with water, 0.1 M, 0.5 M and 1 M NaOH (filled symbols) or KOH (empty symbols) solutions equilibrated for three months. The estimated absolute errors are ±0.05 units in the Ca/Si ratios and ± 0.2 in the H_2O/Si ratios of the C-(N,K-)S-H products. The estimate error of $Ca/Si_{C\text{-}S\text{-}H}$ is smaller than 0.05.

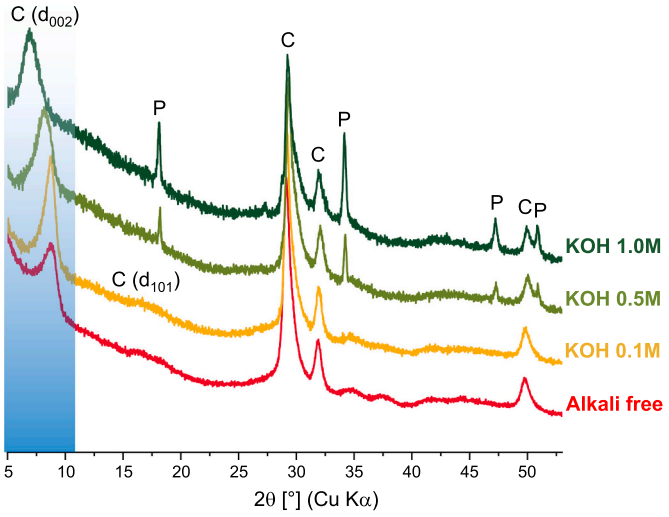

Fig. 9. XRD diffractograms of C-(K-)S-H with target Ca/Si = 1.2 after an equilibration time of 3 months at different KOH concentrations. C: C-(K-)S-H, P: portlandite.

of the basal spacing. Such an increase of basal spacing has been reported previously [26] for samples where a comparable drying method has been used. In contrast, a decrease of basal spacing in the presence of NaOH has been observed [24] for only shortly (overnight) dried samples, which could indicate a faster drying at high NaOH concentrations. The presence of KOH also leads to a decrease of the intensity of the (101) reflection at ≈ 5 Å (16°2θ). The absence of the (101) reflection at 0.5 and 1 M KOH suggests a decreased occupancy of the Si bridging sites at higher alkali concentrations and thus the presence of more Si dimers, as further confirmed by ^{29}Si NMR, FTIR, and Raman data and in good agreement with the decrease of the amount of Q^2 species observed by ^{29}Si NMR for the sample with Ca/Si = 1.0 synthesized in the presence of NaOH [19,27,36].

The positions of the (002) reflections in Fig. 9 correspond to average basal spacings of 9.6 to 15.4 Å for the C-(N, K-)S-H products as summarized in Fig. 10. The variations in the basal spacing are related to drying and the amount of alkali and calcium in the interlayer, with lower interlayer distances at high Ca/Si and an increase at higher alkali contents. The variation in basal spacing could also be due to the presence of different C-(N,K-)S-H products, i.e. poorly-ordered structural analogues of orthorhombic 14 Å tobermorite (PDF# 00-029-0331), 11 Å tobermorite (PDF# 04-017-1028), 9 Å tobermorite (PDF# 04-012-1761), a mixture of these minerals [15] or monoclinic clinotobermorite (PDF# 01-088-1328) [15]. It needs to be emphasized that some samples synthesized in 1 M alkali hydroxide contain two separate basal peaks, which indicates the interstratification of C-S-H layers [63] and/or the presence of different analogues. The profile fitting and the crystallite size refinement for these samples give larger uncertainties.

For alkali-free and low-alkali C-S-H materials, basal space decreases with increasing Ca/Si. The reason of this reduction of interlayer distance could be the charge balance or the attraction effect of the Ca^{2+} in the interlayer [5,18,81]. XRD indicates that the presence of KOH and NaOH increases the mean basal spacing of the C-(N,K-)-S-H as shown in Fig. 10 and in fact, density function theory (DFT) calculations indicate a decrease of attractive forces between the layers upon replacement of Ca^{2+} in the interlayer of C-S-H by Na^{+} [36].

Although at Ca/Si ratios ≥1.0, only a small amount of alkali uptake occurs, the small quantity of KOH or NaOH affects strongly the basal spacing of C-(N, K-)S-H, which underlines that this increase is mainly caused by the removal of Ca^{2+} at high alkali hydroxide and thus low calcium concentrations.

Bach et al. [24] and L'Hôpital et al. [26] reported the decrease of the mean basal spacing in the presence of increasing amounts of NaOH, while the opposite was observed in Fig. 11 (a). The main reason for this inconsistency is that [24] and [26] focused on alkali hydroxide concentrations lower than 0.1 M, where we also observe a slight decrease. However, from 0.1 to 1 M KOH or NaOH concentration, the basal spacing increased from ≈ 10 to ≈ 13 Å, as shown in Fig. 11 (a). At equal concentrations, K and Na have a similar effect of changing the mean basal spacing. This is consistent with L'Hôpital et al. [26], but in contrast to the study of Bach et al. [24], who observed a stronger decrease of the mean basal spacing in the presence of NaOH than of KOH. The reasons for these contradictory observations are unclear, although they might be

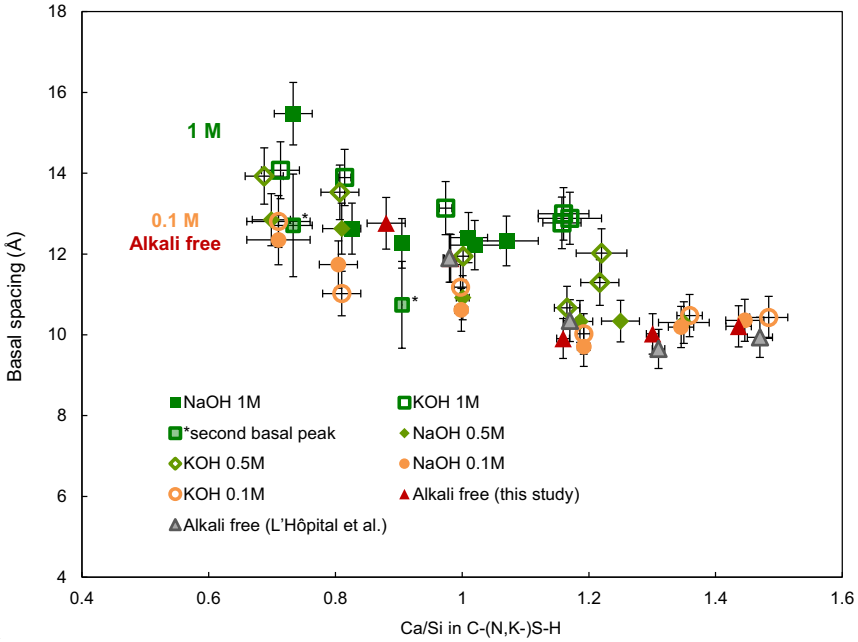

Fig. 10. Variation of the mean basal spacing as a function of the total Ca/Si ratio in C-(N,K-)S-H solid after an equilibration time of 3 months. Grey symbol: C-S-H from L'Hôpital [18]; colored symbol: C-(N,K-)S-H from this study; triangles: C-S-H with water; circles: C-(N,K-)S-H with 0.1 M alkali hydroxide solution, squares: C-(N,K-)S-H with 1 M alkali hydroxide solution; filled symbols: C-(N,K-)S-H with NaOH solution; empty symbols: C-(N,K-)S-H with KOH solution.

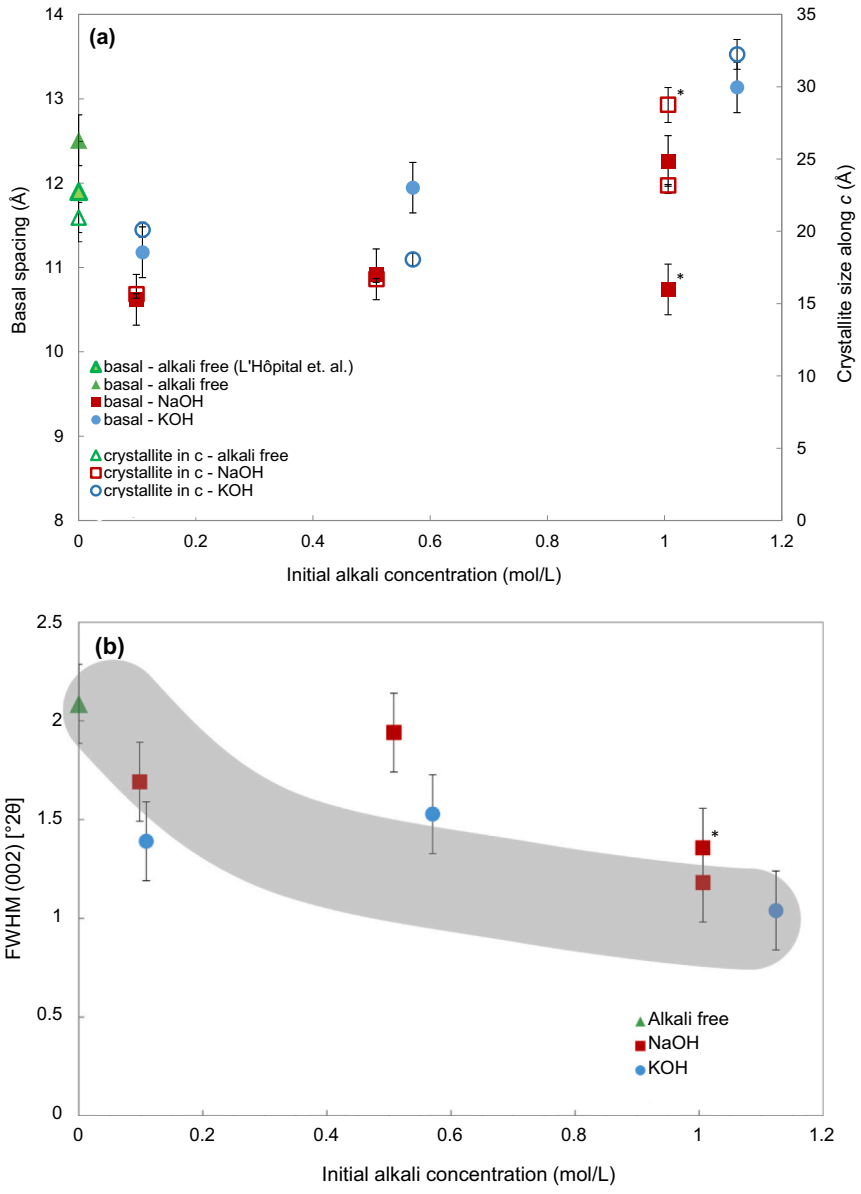

Fig. 11. (a) Variation of mean basal spacing and crystallite size along the c-axis as a function of the initial alkali concentration for C-S-H with Ca/Si = 1.0 after an equilibration time of 3 months, solid symbols: mean basal spacing, empty symbol: crystallite size calculated based on the tobermorite model. Grey symbols: C-S-H from L'Hôpital et al. [18]; colored symbol: C-S-H from this study; triangle. (b) FWHM of the d_{002} reflection of C-(N,K-)S-H with target Ca/Si = 1.0 as a function of initial alkali concentration after an equilibration time of 3 months. Triangles: C-S-H synthesized with water, squares: C-(N, K-)S-H synthesized with NaOH solutions, circles: C-(N, K-)S-H synthesized with KOH solutions. The symbol marked with * stands for the second basal peak. The grey region is shown only as an eye-guide.

related to different washing and drying procedures of the solids, and the shorter equilibration times used in [24].

The crystallite size was estimated from the X-ray diffraction data using a Pawley fit from the unit cells of tobermorite 11 Å [52] and tobermorite 14 Å (for 1.1 M KOH) [54]. An anisotropic crystallite size refinement with two domain lengths (one for the *a*- and *b*-directions, and one for the c-axis direction) is conducted. The fits are given in Fig. A5. The refinement results, presented in Table 2, show that the C-S-H has a much larger crystallite size along the *ab*-axes than along the *c*-axis, which verifies the poorly ordered nature of C-S-H along the *c*-axis, in agreement with earlier studies [8,82]. A crystallite size in the *c* direction of $l_c \approx 15$ Å to 32 Å is observed, denoting 1.5 to 3 layers of C-S-H stacking

Table 2
Unit cell parameters and domain sizes along the a-, and b-axes (l_a) and the c-axis (l_c) obtained from the Pawley fits in Fig. A5 for the different alkali concentrations of C-(N,K-)S-H powder patterns with $Ca/Si_{target} = 1.0$. For the 1.0 M NaOH concentration, two tobermorite unit-cells were used, which differ only in the c-axis length and domain size.

Alkali concentration	*a*	*b*	*c*	*γ*	*V*	l_a	l_c	
	(M)	(Å)	(Å)	(Å)	(°)	(Å^3)	(nm)	(nm)
	0	6.405(2)	7.667(3)	24.10(3)	122.76(4)	995.2(13)	15(3)	2.10(10)
KOH	0.1	6.454(5)	7.799(13)	22.282(17)	123.72(7)	933(2)	10.5(12)	2.01(5)
	0.6	6.441(2)	7.760(6)	23.546(18)	123.41(5)	982.4(13)	9.9(5)	1.81(4)
	1.1	6.464(5)	7.642(6)	26.071(16)	123.18(7)	1077.8(16)	9.0(14)	3.14(9)
NaOH	0.1	6.404(5)	7.871(9)	21.417(14)	123.52(8)	900.0(16)	8.5(6)	1.57(3)
	0.5	6.417(2)	7.817(5)	21.838(13)	123.45(3)	914.0(9)	13.5(8)	1.67(2)
	1.0	6.442(4)	7.589(7)	23.958(19)	124.27(8)	967.8(16)	11(3)	2.32(6)
	1.0	6.442(4)	7.589(7)	21.01(3)	124.27(8)	848.7(17)	11(3)	2.87(12)

in the *c*-axis. In C-S-H with NaOH 1 M, a shoulder is observed at ~10.7 Å, other than the major basal peak at ~12.3 Å, indicating two major nanocrystalline structures in this sample that share similar structures in *ab*-plane but have different basal spacings.

The relative intensity and width of the (002) reflections are highly sensitive to the crystallite size along the *c*-axis (l_c). A correlation between increasing alkali hydroxide concentration and larger crystallite size in the *c*-direction with smaller crystallite size in the *ab*-plane can be observed for C-S-H with KOH. The trend of smaller crystallite size in *ab*-direction for C-S-H with NaOH is less clear, which may be due to the larger uncertainty from the mixture of tobermorite analogues present. The crystallite size in the *c*-direction and basal spacing follow the same trend along the higher amount alkali hydroxide.

As discussed in previous studies [26,27,36,49], higher alkali hydroxide concentration shortens the silicate chains of C-S-H. So the increased crystallite size can be assumed to stem from an increase along the *c*- axis. Pair distribution function (PDF) calculations of synthetic C-S-H indicated a crystallite size of ≈ 4 nm and no significant variations with the NaOH concentrations up to 5 M [36], but the C-S-H are pre-assumed as identical along *a*-, *b*- and *c*- axes.

Grangeon et al. [63] suggested that a shift of the basal reflection in XRD towards low angles and an increase in its FWHM could indicate fewer stacking layers in the *c* direction. In this study, the basal reflection shifts towards lower angles while the domain size increases (i.e. FWHM decreases) as a function of alkali concentration in C-(Na,K-)S-H, as shown in Fig. 11 (b). The FWHM might include several analogues of tobermorite, giving the larger values for the 0.5 M concentration. The lower angle shifting of basal reflection and decreasing FWHM indicate:

i) an expansion of the interlayer distance, probably related to the replacement of Ca^{2+} by alkali ions in the interlayer [5,26,36,83], which either lowers the attractive forces between the separate layers [36] or brings more water molecules into the interlayer [83]. The latter hypothesis can be explained as more water is associated with two Na^+ and K^+ cations than with one Ca^{2+} cation. The Na^+ or K^+ attracts the water molecule along the direction that is parallel to the silicate chain in C-(N,K-)S-H. The force resulting from this attraction decreases the lateral area (i.e., along the *ab* direction), while simultaneously increasing the length along the *c*-direction (i.e., expanding the interlayer).
ii) an increase in the crystallite size along *c*-axis. One possible interpretation of these phenomena is that alkali hydroxide lowers the degree of silicate polymerization in C-S-H and as a result the C-S-H grows rather in *c*-direction (rather than in the *ab*-direction) resulting in higher number of layers stacked along the *c*-axis.

3.3.4. Composition of C-(N,K-)S-H

The chemical compositions of the C-(N,K-)S-H products formed at different Ca/Si_{target} ratios was calculated by mass balance calculation considering the amount of Ca and Si in the aqueous phase and secondary phases present, only the amount of NaOH and KOH was obtained from direct measurements as detailed above. The variations in the composition of C-S-H are summarized in Fig. 12. The C-(N,K-)S-H products formed in water and 0.1 M NaOH and KOH have Ca/Si ratios between 0.78 and 1.44. In general, the $Ca/Si_{C\text{-}S\text{-}H}$ ratios are similar to the Ca/Si_{target}, due to the relatively low levels of secondary phases formed in these specimen. The samples synthesized with $Ca/Si_{target} = 1.6$ contained portlandite, which lowered the $Ca/Si_{C\text{-}S\text{-}H}$ to slightly below 1.5. The presence of 1 M alkali hydroxide solutions lowered the maximum $Ca/Si_{C\text{-}S\text{-}H}$ of C-(N,K-)S-H to 1.2, as more portlandite is formed at higher pH values (Fig. 9), indicating a strong effect of pH on C-S-H composition under equilibrium conditions. The lowest $Ca/Si_{C\text{-}S\text{-}H}$ is also affected by the presence of alkali hydroxide; the higher pH values increase the Si concentrations, which led to the dissolution of amorphous silica at 0.1 M alkali hydroxide and above, as well as to more Si in solution. The preference of Si to be in solution instead of solid phase results in an decrease of the observed minimum $Ca/Si_{C\text{-}S\text{-}H}$ from 0.75 at alkali free C-S-H to ~0.7 at C-S-H with alkali hydroxide.

3.4. Effect of pH on silica sites in C-S-H

The ^{29}Si MAS NMR spectra of the C-S-H samples with Ca/Si = 1.2 and cured in different KOH concentrations are shown in Fig. 13. Three resonances at approx. -79 ppm (Q^1), −83 ppm (Q_b^2) and − 85 ppm (Q_{pa}^2) are identified for the alkali-free sample, as discussed above.

The presence of KOH shifts the Q^1 and Q^2 peaks to lower frequency as

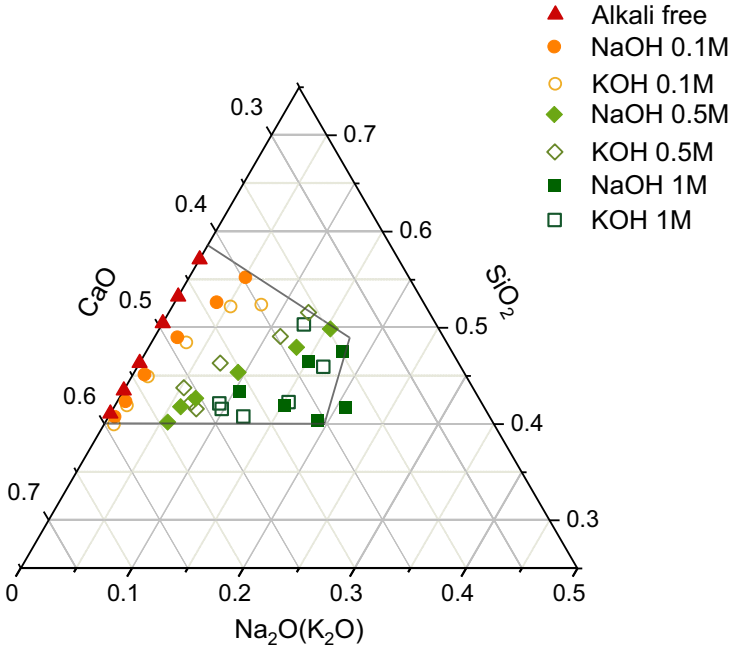

Fig. 12. Chemical compositions (units in molar fraction) of the C-(N, K-) S—H products of different target Ca/Si and with different NaOH or KOH concentration projected in ternary diagram.

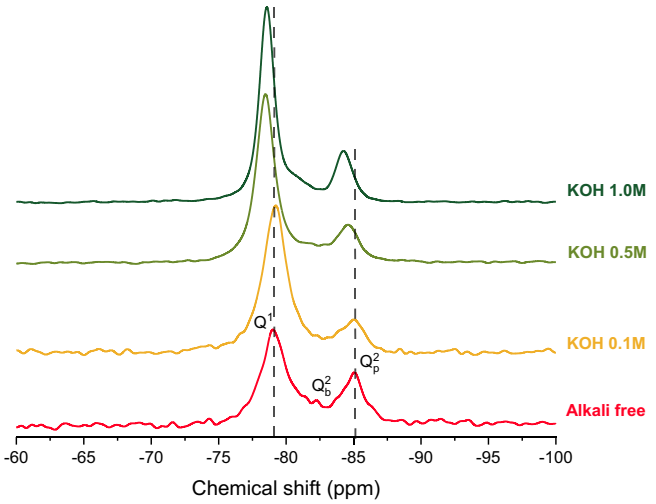

Fig. 13. ^{29}Si NMR spectra of C-(N,K-)S-H a) with Ca/Si$_{target}$ = 1.2 after an equilibration time of 3 months at different KOH concentrations.

a result of the replacement of Ca^{2+} by K^{+} in the interlayer, which contribute to a weaker shielding of the Si atoms as compared to Ca^{2+} [36]. The observed shifts are consistent with earlier observations for C-S-H gels exposed to NaOH and KOH [19,27,36,84] and with the shifts to lower wavenumbers observed in both Raman and FTIR signals at around 1000 cm^{-1} as discussed below.

With increasing KOH or NaOH concentrations, the intensity of the Q^1 signal increases indicating a shortening of the MCL, as also observed in previous studies [27,36]. For the C-S-H samples with Ca/Si$_{target}$ of 1.0 and below, the changes in mean chain length are much more distinct than at 1.2, while at Ca/Si$_{target}$ > 1.2, the mean chain length and silica connectivity is not strongly affected at higher KOH concentrations [5,36,58] since silicate dimers dominate at high Ca/Si.

In addition, small amounts (< 3%) of Q^0 peaks (−70 ppm) were observed for the C-S-H samples synthesized in 1 M NaOH at Ca/Si$_{target}$ values of 0.6 to 1.6 and in 1 M KOH at Ca/Si$_{target}$ 0.8 (see Fig. A4). The Q^0 peaks are assigned to hydrated monomeric silicate species in the solid following the assignment of Garg et al. [36]. For C-S-H synthesized in 1 M alkali hydroxide, these Q^0 units are possibly charge-balanced by the high levels of alkalis. It should be noted that from a thermodynamic stability point of view, an excess of depolymerized Q^0 silicate units are

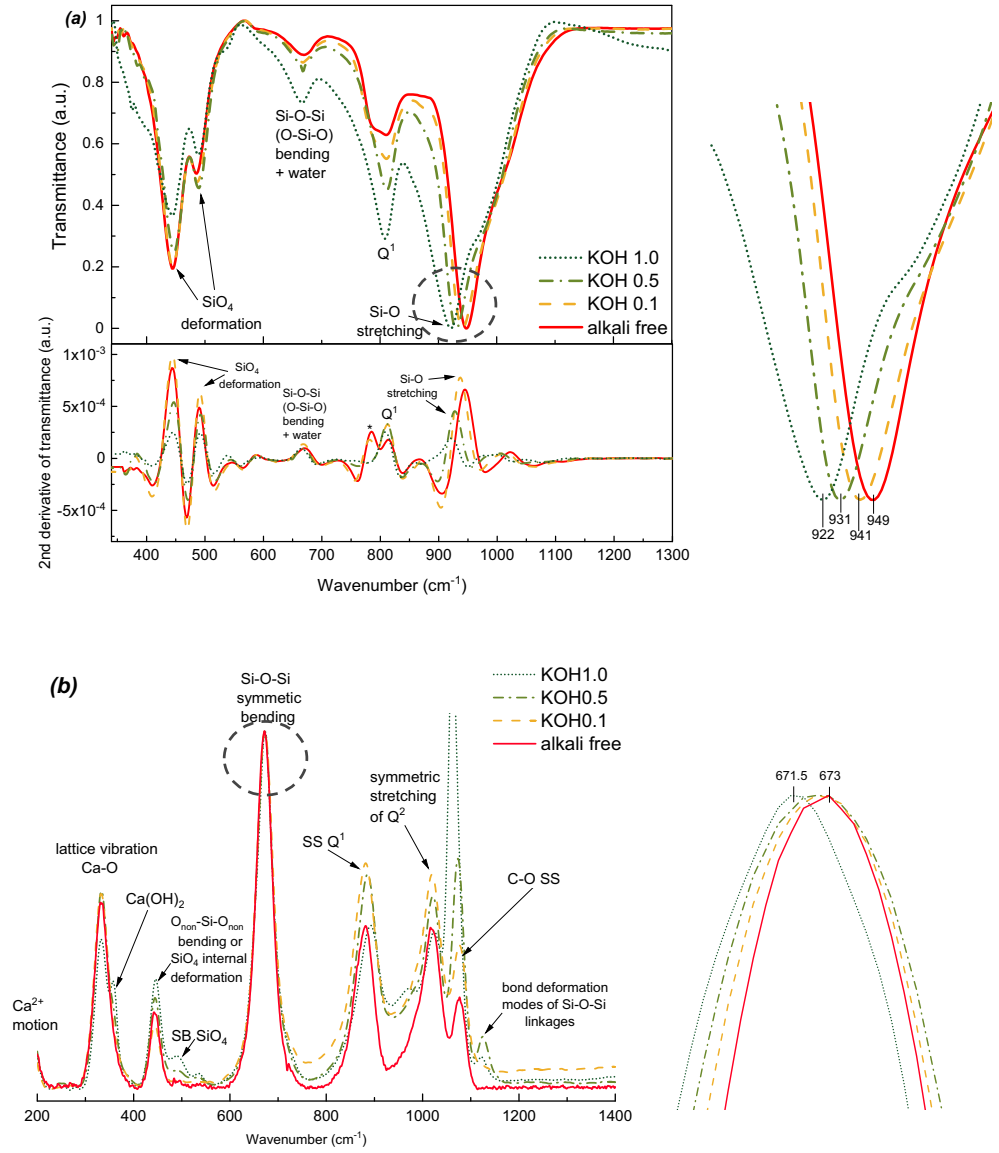

Fig. 14. (a) FTIR and (b) Raman spectra of C-(N,K-)S-H with target Ca/Si = 1.2 after an equilibration time of 3 months at different KOH concentrations.

preferable dissolved [36].

Fig. 14 shows the effect of KOH on the FTIR and Raman spectra of C-(K-)S-H with $Ca/Si_{target} = 1.2$. The main FTIR peak at 960 cm^{-1} is shifted to lower wavenumbers (redshift) confirming the depolymerisation of the silica chains [46]. This peak splits into two peaks at higher KOH concentrations indicating a lowering of the symmetry resulting from the transformation of structural sites into groups of non-equivalents sites [47]. The peak splitting has also been observed to a limited extent at higher Ca/Si_{target} and much more distinct at low Ca/Si_{target} (see Fig. A3). This lower symmetry indicated peak split could be due to the substitution of Ca^{2+} by K^{+} in the interlayer, i.e. by the changes in the second coordination sphere. The shift to lower wavenumber indicates a structural rearrangement of C-S-H in the presence of KOH, for example a change in Si—O bond distances and/or the Si-O-Si angles [64]. In the Raman spectra a similar shift of the main peak related to Si-O-Si symmetric bending from 671.5 to 673 cm^{-1} occurs, which indicates the value of the angle < Si-O-Si > decreases in the presence of KOH [70]. Also the appearance of small peak at ~1120 cm^{-1} Raman spectra indicates increasing bond deformation of Si-O-Si linkages [61].

The Q^1 signal is located at ~815 cm^{-1} in FTIR and ~ 882 cm^{-1} in Raman. The intensity of the Q^1 signal in FTIR increases indicating the presence of more Q^1 silica and thus a shortening of the silica chain length, in agreement with the observations by Si-NMR. Also in Raman, the intensity of the SS Q^1 increases from alkali free to 0.5 M KOH indicating a shorter MCL. The SS Q^1 peak at 1 M KOH, however, does not follow the expected trend. During sample preparation and measurement a slight carbonation of the surface occurred, which led to a C-S-H decalcification and silica polymerization and diminishment of the SS Q^1 intensity [60] at the surface of the samples, although the bulk C-S-H show very little weight loss from 600 to 900 °C in Fig. 7. The carbonation is in particularly well visible in the Raman peaks at 1080 cm^{-1}, which are attributed to the C—O SS vibration of carbonation [69–71,73] and strongly affect the intensity of the Si—O SS of C-S-H at ~1020 cm^{-1}. The carbonate peak at ~1077 cm^{-1} increasingly dominates the spectra of C-S-H with KOH, which is attributed to the symmetric stretching mode of vaterite [60]. The fast carbonation of the samples surface at high pH values and high $Ca/Si_{C\text{-}S\text{-}H}$ makes the interpretation of the Raman signals very challenging.

The addition of KOH increases the intensity of the FTIR band at 670 cm^{-1}, which has been related to Si-O-Si (O-Si-O) bending [46,65] and water liberations [65]. This increase has been observed at all Ca/Si ratios (see Fig. A3) and could thus be related to the presence of additional water. The FTIR spectral range 2500-4000 cm^{-1} in Fig. A2 shows that the intensity of the water signal is significantly higher at 1 M KOH than for the other samples indicating the presence of more loosely bound water in agreement with the TGA results.

In addition, in FTIR the peak at 450 cm^{-1} and a peak at 490 cm^{-1} are increasing, which has been assigned to internal deformation of the Si-tetrahedra [69] or O-Si-O bending [70] and symmetric bending vibrations of SiO_4 [69–71]. As discussed in Fig. 3(c) the peak at 780 cm^{-1} is also observed and disappears at higher alkali concentrations. In Raman, the addition of KOH did not change the peak intensity Ca—O lattice vibrations at 325 cm^{-1} did not change except for 1 M KOH, which could be related to the formation of more portlandite.

The XRD, NMR, FTIR and Raman data all indicate the formation of shorter silica chains in the presence of more KOH and NaOH, which agrees with the decrease of MCL predicted based on thermodynamic modelling using the CASH+ model in Fig. 15. In agreement with the experiments (the MCL calculated from NMR and secondary phases are

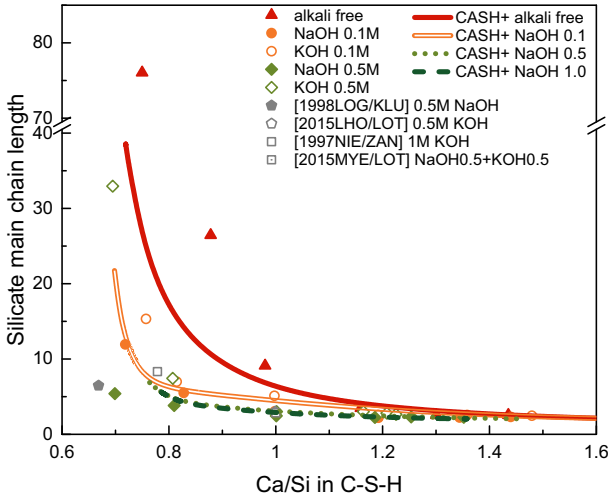

Fig. 15. Calculated main chain length (MCL) of C-(N,K-)S-H from Gems compared with MCL values reported from ^{29}Si NMR. The estimated absolute errors are less than 30%. The error limits for the MCL from NMR is ±0.05. Solid and empty symbols: MCL from NMR; red triangles: C-S-H with MilliQ water; orange circles: C-(N,K-)S-H with 0.1 M alkali hydroxide solution, light green diamonds: C-(N,K-)S-H with 0.5 M alkali hydroxide solution, grey symbols: C-(N,K-)S-H with 0.5 M – 1 M alkali hydroxide solution adapted from [19,27,84,85]. Lines: simulated using the thermodynamic CASH+ model. (For interpretation of the references to colour in this figure legend, the reader is referred to the web version of this article.)

presented in Table A3), the presence of alkali hydroxide decreases the MCL in C-S-H due to the removal of Si from the bridging sites at higher pH values, due to the increasing tendency of negatively charged Si species ($SiH_3O_4^-$ and $SiH_2O_4^{-2}$) to be solution at higher pH values. In addition, higher pH values increase the deprotonation of $\equiv SiO^-$ surface groups in C-S-H [25,26,28,31,32,76], which increases the negative surface and interlayer charge of C-S-H and thus lowers the tendency of silicon to bind on bridging sites.

4. Conclusions

The effect of Ca/Si and the influence of KOH and NaOH on the structure and solubility of C-S-H has been studied. An increase of Ca/Si_{target} led to lower Si concentrations, to higher Ca concentrations and higher pH values in the surrounding solutions. In parallel to the solution composition, the composition and structure of the C-S-H varied from $Ca/Si_{C\text{-}S\text{-}H} = 0.75$ in the presence of amorphous SiO_2 to $Ca/Si_{C\text{-}S\text{-}H} = 1.44$ in the presence of portlandite, while the chain length of the silica chains decreased from >70 to mainly dimers at $Ca/Si_{C\text{-}S\text{-}H} = 1.3$ and above. The MCLs quantified from the FTIR and Raman spectra agrees well with the results from ^{29}Si NMR, indicating that a reliable qualitative analysis is also possible based on FTIR and Raman. However, the Raman results were very sensitive to any surface carbonation occurring during the measurement, which would make them unsuitable for quantification. The disappearance of the bridging silica tetrahedra could also be observed by the disappearance of the XRD d_{101} peak. A shift of the main Si—O stretching signal in FTIR to lower wavenumbers confirmed the depolymerisation of the silicate chains. XRD indicates a decrease of the interlayer distances at higher $Ca/Si_{C\text{-}S\text{-}H}$ ratios, where more Ca^{2+} is in the interlayer, which increases the cohesion between the negatively charged

main layers.

The presence of KOH and NaOH had a similar effect on both the aqueous phase and solid phase. The addition of KOH or NaOH increased the pH values and the Si concentrations and lowered the Ca concentrations in solution. The precipitation of additional portlandite at high pH values as well as the increased Si concentrations due to the preference of Si to form negatively charged complexes lead to a decreases of $Ca/Si_{C\text{-}S\text{-}H}$ from 1.44 in the absence of NaOH to $Ca/Si_{C\text{-}S\text{-}H} \approx 1.1$ in the presence of 1 M NaOH or KOH. The uptake of alkali in C-S-H was higher at low Ca/Si as well as at higher pH values, as both the lower Ca-concentration and increased deprotonation of the silanol group $\equiv SiO^-$ surface at higher pH contribute to an increased alkali binding by C-S-H in agreement with the prediction of the thermodynamic model. Higher concentration of alkali hydroxide also prevented the polymerization of C-(N,K-)S-H silicate as indicated by NMR, FTIR and Raman spectroscopy and increased the crystallite size along the *c*-axis from ≈16 Å in 0.1 M KOH to 31 Å in 1.1 M KOH after 3 months of curing at 20 °C degree.

This study for the first time combined a series of spectroscopy methods including NMR, FTIR and Raman to study the effect of alkali hydroxide on the structure of C-S-H. With the help of the Si NMR data, we assigned clearly the vibration bands of C-S-H in FTIR and Raman. The data showed that it is possible to use FTIR and Raman as heuristic tools to quantify the MCL, and it showed good qualitative agreements with the MCL from NMR. In addition, we observed the C-S-H composition change as a function of alkali hydroxide concentration, where the upper limit decreases of the $Ca/Si_{C\text{-}S\text{-}H}$ from ~1.44 (no alkali) to 1.1 (1M KOH/NaOH), and the lower limit from 0.75(no alkali) to ~0.7 in the presence of alkali hydroxide. The comparison with the independently developed CASH+ thermodynamic model showed that the model reproduced the observed changes, including the shortening of the MCL in the presence of NaOH and KOH. This study adds important data to improve the thermodynamic modelling and the insights into the composition and structure relationship of C-(N,K-)S-H, which are expected to contribute our understanding on the effect of alkali hydroxides on C-S-H.

Declaration of competing interest

The authors declare that they have no known competing financial interests or personal relationships that could have appeared to influence the work reported in this paper.

Acknowledgements

Financial support from the Swiss National Foundation (SNF) (Project No. 200021_169014) and the Danish Council for Independent Research, Technology and Production (No. 7017-00092) are gratefully acknowledged. The authors would like to thank Luigi Brunetti and Bin Ma for support to measure elemental concentration of the solution, Andreas Borgschulte and Beatrice Fischer for the help with Raman and FTIR measurements, Boris Ingold and Luigi Brunetti for the lab support. Malene Thostrup Pedersen, Andreas Leemann, Bin Ma, Zhangli Hu, Ellina Bernard, Biwan Xu and Zhenguo Shi are acknowledged for helpful discussions.

CRediT authorship contribution statement

Y. Yan. and B. Lothenbach. conceived and designed the experiments. Y. Yan. S. Y. Yang and E. L'Hôpital conducted the experiments. G. D. Miron supported the thermodynamic modelling, J. Skibsted supported the NMR interpretation, I. E. Collings and F. Winnefeld supported crystallite size fittings and the X-ray diffraction interpretation. K. Scrivener and B. Lothenbach supervised this work. All authors reviewed the manuscript.

Appendix A

Table A1
Aqueous dissolved concentrations and pH results for the C-(N, K-)S-H samples.

Synthesis solution	[Si] (mM)	[Ca] (mM)	[K] (mM)	[Na] (mM)	[OH-] (mM)	pH[a]
Ca/Si* = 0.6						
Water	3.84	1.23	0	0	0.19	9.9
0.1 M NaOH	29.2	0.01	0	46.2	16.6	12.2
0.1 M KOH	26.5	b.d.l	50.1	0	23.0	12.3
0.5 M NaOH	33.5	b.d.l	0	440	418	13.5
0.5 M KOH	30.3	0.02	462	0	404	13.5
1 M NaOH	43.1	0.01	0	944	868	13.9
1 M KOH	37.5	0.01	1082	0	871	13.8
Ca/Si* = 0.8						
Water	1.60	0.91	0	0	0.65	10.5
0.1 M NaOH	1.20	0.04	0	61.0	97.1	12.9
0.1 M KOH	1.13	0.03	67.5	0	59.0	12.7
0.5 M NaOH	2.59	0.01	0	437	418	13.5
0.5 M KOH	1.88	0.05	467	0	388	13.5
1 M NaOH	6.63	0.02	0	937	839	13.8
1 M KOH	3.87	0.04	1074	0	937	13.8
Ca/Si* = 1.0						
Water	0.07	3.50	0	0	9.2	11.7
0.1 M NaOH	0.15	0.40	0	78.7	101	13.0
0.1 M KOH	0.14	0.44	85.9	0	75.4	12.8
0.5 M NaOH	0.36	0.15	0	472	406	13.5

(*continued on next page*)

Table A1 (*continued*)

Synthesis solution	[Si] (mM)	[Ca] (mM)	[K] (mM)	[Na] (mM)	[OH-] (mM)	pH[a]
0.5 M KOH	0.55	0.15	501	0	457	13.5
1 M NaOH	0.47	0.22	0	978	839	13.8
1 M KOH	0.71	0.32	1081	0	937	13.8
Ca/Si* = 1.2						
Water	0.01	7.11	0	0	16.9	12.0
0.1 M NaOH	b.d.l	1.39	0	94.0	97.1	12.9
0.1 M KOH	0.03	1.34	101	0	88.8	12.9
0.5 M NaOH	b.d.l	0.85	0	495	422	13.5
0.5 M KOH	0.10	0.77	515	0	476	13.5
1 M NaOH	0.18	0.47	0	968	899	13.9
1 M KOH	0.51	0.54	1108	0	937	13.8
Ca/Si* = 1.4						
Water	0.01	16.0	0	0	51.4	12.4
0.1 M NaOH	b.d.l	4.45	0	93.3	97.1	12.9
0.1 M KOH	0.01	4.17	102	0	92.5	12.9
0.5 M NaOH	b.d.l	0.98	0	486	455	13.6
0.5 M KOH	0.09	0.88	516	0	496	13.6
1 M NaOH	0.13	0.56	0	980	839	13.8
1 M KOH	0.45	0.61	1104	0	972	13.8
Ca/Si* = 1.6						
Water	b.d.l	21.3	0	0	55.2	12.5
0.1 M NaOH	b.d.l	5.09	0	94.1	122	13.0
0.1 M KOH	0.01	4.72	1123	0	129	13.0
0.5 M NaOH	b.d.l	1.11	0	498	472	13.6
0.5 M KOH	0.09	0.94	514	0	476	13.5
1 M NaOH	0.11	0.61	0	990	868	13.9
1 M KOH	0.43	0.63	1102	0	972	13.8

[a] pH measured at ~24 °C.

Table A2
Chemical compositions of the C-(N,K-)S-H products, determined from IC, TGA, XRD and pH measurements, The estimated absolute errors are less than ±0.05 units in the Ca/Si ratios, ±0.2 units in the H_2O/Si ratios, and ±0.05 units for the 0.1 M alkali samples in the (Na/ K)/Si ratios of the C-(N,K-)S-H products. Ca/Si* = target Ca/Si.

Synthesis solution	C-(N,K-)S-H chemical formula	$Ca/Si_{C\text{-}S\text{-}H}$	Na/Si[c]	K/Si[c]	H_2O/Si
Ca/Si* = 0.6					
Water	$(CaO)_{0.78}SiO_2(H_2O)_{1.2}$[a]	0.78[a]	-	-	1.21
0.1 M NaOH	$(CaO)_{0.71}(Na_2O)_{0.13}SiO_2(H_2O)_{1.0}$	0.71	0.21	-	1.04
0.1 M KOH	$(CaO)_{0.71}(K_2O)_{0.14}SiO_2(H_2O)_{1.1}$	0.71	-	0.27	1.13
0.5 M NaOH	$(CaO)_{0.70}(Na_2O)_{0.65}SiO_2(H_2O)_{1.4}$	0.70	0.65[c]	-	1.38
0.5 M KOH	$(CaO)_{0.69}(K_2O)_{0.48}SiO_2(H_2O)_{1.3}$	0.69	-	0.48	1.35
1.0 M NaOH	$(CaO)_{0.73}(Na_2O)_{0.76}SiO_2(H_2O)_{1.9}$	0.73	0.76	-	1.86
1.0 M KOH	$(CaO)_{0.73}(K_2O)_{0.49}SiO_2(H_2O)_{1.3}$	0.73	-	0.49	1.30
Ca/Si* = 0.8					
Water	$(CaO)_{0.88}SiO_2(H_2O)_{1.3}$	0.88	-	-	1.32
0.1 M NaOH	$(CaO)_{0.81}(Na_2O)_{0.17}SiO_2(H_2O)_{1.1}$	0.81	0.17	-	1.10
0.1 M KOH	$(CaO)_{0.83}(K_2O)_{0.20}SiO_2(H_2O)_{1.2}$	0.83	-	0.20	1.24
0.5 M NaOH	$(CaO)_{0.81}(Na_2O)_{0.56}SiO_2(H_2O)_{1.7}$	0.81	0.56	-	1.66
0.5 M KOH	$(CaO)_{0.81}(K_2O)_{0.46}SiO_2(H_2O)_{1.6}$	0.81	-	0.46	1.55
1.0 M NaOH	$(CaO)_{0.83}(Na_2O)_{0.67}SiO_2(H_2O)_{1.9}$	0.83	0.67	-	1.90
1.0 M KOH	$(CaO)_{0.81}(K_2O)_{0.73}SiO_2(H_2O)_{1.8}$	0.81	-	0.73	1.75
Ca/Si* = 1.0					
Water	$(CaO)_{0.98}SiO_2(H_2O)_{1.5}$	0.98	-	-	1.48
0.1 M NaOH	$(CaO)_{1.00}(Na_2O)_{0.10}SiO_2(H_2O)_{1.1}$	1.00	0.10	-	1.14
0.1 M KOH	$(CaO)_{1.00}(K_2O)_{0.13}SiO_2(H_2O)_{1.5}$	1.00	-	0.13	1.47
0.5 M NaOH	$(CaO)_{1.00}(Na_2O)_{0.43}SiO_2(H_2O)_{1.5}$	1.00	0.43	-	1.46
0.5 M KOH	$(CaO)_{1.00}(K_2O)_{0.31}SiO_2(H_2O)_{1.6}$	1.00	-	0.31	1.61
1.0 M NaOH	$(CaO)_{0.90}(Na_2O)_{1.12}SiO_2(H_2O)_{2.1}$	0.90[b]	1.12	-	2.10
1.0 M KOH	$(CaO)_{1.00}(K_2O)_{0.73}SiO_2(H_2O)_{2.4}$	0.97	-	0.73	2.38

(*continued on next page*)

Table A2 (*continued*)

Synthesis solution	C-(N,K-)S-H chemical formula	$Ca/Si_{C\text{-}S\text{-}H}$	Na/Si[c]	K/Si[c]	H_2O/Si
Ca/Si* = 1.2					
Water	$(CaO)_{1.16}SiO_2(H_2O)_{1.4}$	1.16	-	-	1.37
0.1 M NaOH	$(CaO)_{1.19}(Na_2O)_{0.06}SiO_2(H_2O)_{1.3}$	1.19	0.06	-	1.28
0.1 M KOH	$(CaO)_{1.19}(K_2O)_{0.06}SiO_2(H_2O)_{1.4}$	1.19	-	0.06	1.38
0.5 M NaOH	$(CaO)_{1.19}(Na_2O)_{0.34}SiO_2(H_2O)_{1.5}$	1.19[b]	0.34	-	1.51
0.5 M KOH	$(CaO)_{1.16}(K_2O)_{0.24}SiO_2(H_2O)_{1.6}$	1.16[b]	-	0.24	1.62
1.0 M NaOH	$(CaO)_{1.01}(Na_2O)_{1.02}SiO_2(H_2O)_{2.5}$	1.01[b]	1.02	-	2.49
1.0 M KOH	$(CaO)_{1.16}(K_2O)_{0.44}SiO_2(H_2O)_{1.8}$	1.16[b]	-	0.44	1.82
Ca/Si* = 1.4					
Water	$(CaO)_{1.30}SiO_2(H_2O)_{1.5}$	1.30	-	-	1.47
0.1 M NaOH	$(CaO)_{1.34}(Na_2O)_{0.04}SiO_2(H_2O)_{1.5}$	1.34[b]	0.04	-	1.46
0.1 M KOH	$(CaO)_{1.36}SiO_2(H_2O)_{1.6}$	1.36[b]	-	-	1.61
0.5 M NaOH	$(CaO)_{1.25}(Na_2O)_{0.32}SiO_2(H_2O)_{1.5}$	1.25[b]	0.32	-	1.53
0.5 M KOH	$(CaO)_{1.21}(K_2O)_{0.32}SiO_2(H_2O)_{2.0}$	1.21[b]	-	0.32	1.96
1.0 M NaOH	$(CaO)_{1.02}(Na_2O)_{0.85}SiO_2(H_2O)_{2.3}$	1.02[b]	0.85	–	2.29
1.0 M KOH	$(CaO)_{1.16}(K_2O)_{0.60}SiO_2(H_2O)_{2.2}$	1.16[b]	–	0.60	2.24
Ca/Si* = 1.6					
Water	$(CaO)_{1.44}SiO_2(H_2O)_{1.6}$	1.44[b]	–	–	1.60
0.1 M NaOH	$(CaO)_{1.44}(Na_2O)_{0.03}SiO_2(H_2O)_{1.6}$	1.44[b]	0.03	–	1.56
0.1 M KOH	$(CaO)_{1.48}SiO_2(H_2O)_{1.7}$	1.48[b]	–	–	1.73
0.5 M NaOH	$(CaO)_{1.35}(Na_2O)_{0.31}SiO_2(H_2O)_{1.6}$	1.35[b]	0.31	–	1.59
0.5 M KOH	$(CaO)_{1.22}(K_2O)_{0.36}SiO_2(H_2O)_{2.4}$	1.22[b]	–	0.36	2.40
1.0 M NaOH	$(CaO)_{1.07}(Na_2O)_{0.54}SiO_2(H_2O)_{2.2}$	1.07[b]	0.54	–	2.19
1.0 M KOH	$(CaO)_{1.17}(K_2O)_{0.47}SiO_2(H_2O)_{2.4}$	1.17[b]	–	0.47	2.37

- = not applicable: as no Na or K was added during synthesis (<0.6 mM Na is present as an impurity in the 0.1 M KOH synthesis solution).

[a] Lowered due to the presence of SiO_2 as indicated by NMR and saturation indices with respect to SiO_2.

[b] Portlandite present in addition to C-S-H.

[c] Alkali/Si ratios based on direct methods [26] are associated with an error of ±0.2 units for the 0.5 M alkali samples and ± 0.7 for the 1 M alkali samples.

Table A3
Secondary phase quantification and mean silica chain length (MCL) of C-S-H samples without and with alkali hydroxide.

Synthesis solution	$Ca/Si_{C\text{-}S\text{-}H}$	SiO_2 amorphous (wt%)	Portlandite (wt%)	$K_2CO_3 \cdot 1.5H_2O$ (wt%)	MCL
Ca/Si* = 0.6					
Water	0.75[a]	10.1			76.1
0.1 M NaOH	0.71	2.22			11.9
0.1 M KOH	0.71	4.84			15.3
0.5 M NaOH	0.70				5.41
0.5 M KOH	0.69	0.42			33.0
1 M NaOH	0.73				
1 M KOH	0.73	1.28			
Ca/Si* = 0.8					
Water	0.88	4.05			26.5
0.1 M NaOH	0.81	1.27			5.50
0.1 M KOH	0.83	0.53			6.99
0.5 M NaOH	0.81				3.82
0.5 M KOH	0.81				7.44
1 M NaOH	0.83				
1 M KOH	0.81				
Ca/Si* = 1.0					
Water	0.98				9.12
0.1 M NaOH	1.00				3.06
0.1 M KOH	1.00				5.11
0.5 M NaOH	1.00				2.46
0.5 M KOH	1.00				3.01
1 M NaOH	0.90[b]		4.69		
1 M KOH	0.97		0.85	4.65	
Ca/Si* = 1.2					
Water	1.16				3.48

(*continued on next page*)

Table A3 (*continued*)

Synthesis solution	$Ca/Si_{C\text{-}S\text{-}H}$	SiO_2 amorphous (wt%)	Portlandite (wt%)	$K_2CO_3 \cdot 1.5H_2O$ (wt%)	MCL
0.1 M NaOH	1.19				2.20
0.1 M KOH	1.19				2.56
0.5 M NaOH	1.19[b]		0.44		2.24
0.5 M KOH	1.16[b]		1.42		3.01
1 M NaOH	1.01[b]		7.83		
1 M KOH	1.16[b]		2.05		
Ca/Si* = 1.4					
Water	1.30				2.55
0.1 M NaOH	1.34[b]		1.27		2.22
0.1 M KOH	1.36[b]		0.75		2.56
0.5 M NaOH	1.25[b]		6.09		2.31
0.5 M KOH	1.21[b]		7.21		2.80
1 M NaOH	1.02[b]		14.9		
1 M KOH	1.16[b]		9.70		
Ca/Si* = 1.6					
Water	1.44[b]				2.56
0.1 M NaOH	1.44[b]		5.27		2.30
0.1 M KOH	1.48[b]		3.72		2.47
0.5 M NaOH	1.35[b]		9.87		2.26
0.5 M KOH	1.22[b]		12.8		2.64
1 M NaOH	1.07[b]		20.3		
1 M KOH	1.17[b]		15.8		

* Amorphous SiO_2 and MCL quantified from ^{29}Si NMR. Portlandite quantified by TGA.

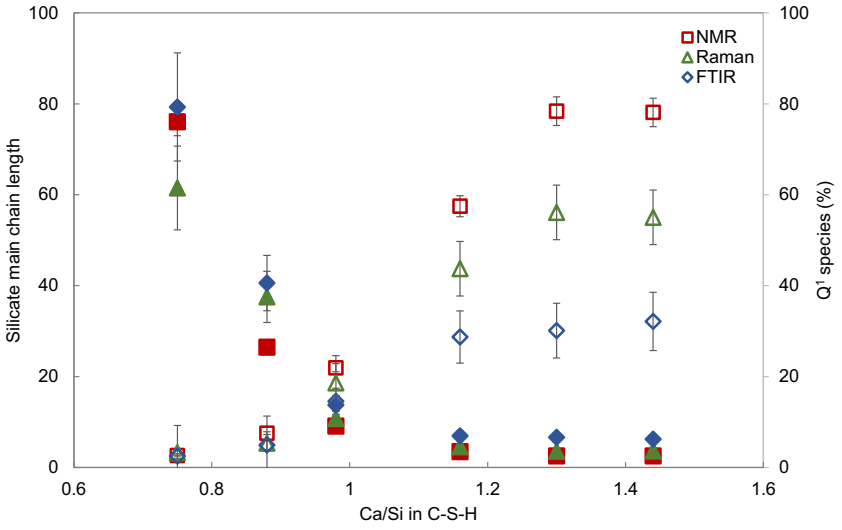

Fig. A1. Silicate main chain length and Q^1 species determined by FTIR, Raman and ^{29}Si NMR and thermodynamic CASH+ model. Filled symbols: silicate main chain length, empty symbols: Q1 species.

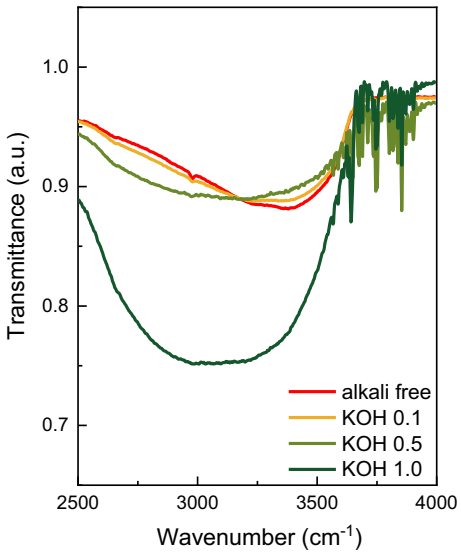

Fig. A2. FTIR spectra water region of C-(N,K-)S-H with target Ca/Si = 1.2 after an equilibration time of 3 months at different KOH concentrations.

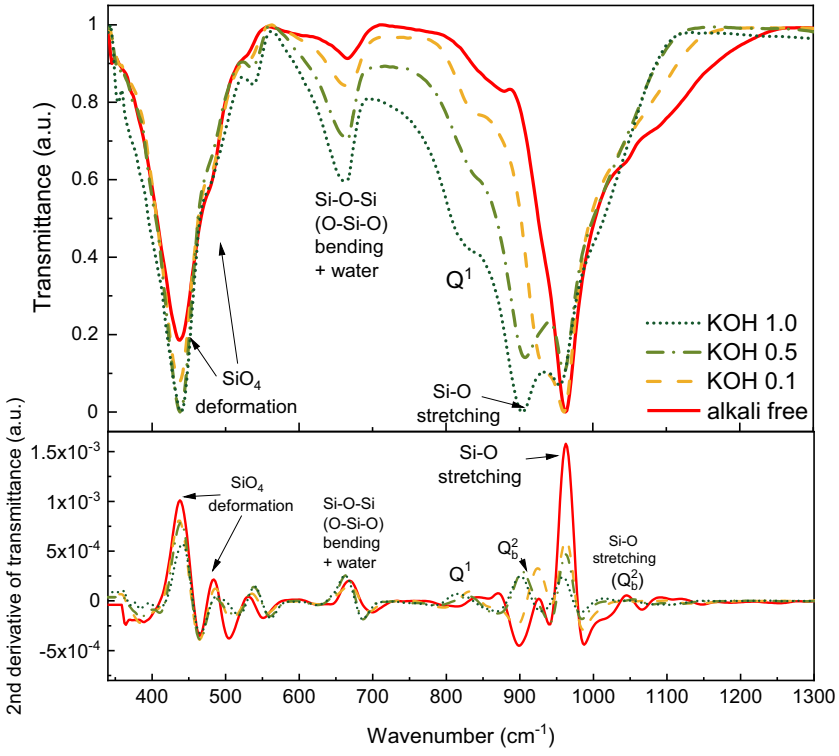

Fig. A3. FTIR spectra of C-(N,K-)S-H with Ca/Si_{target} = 0.6 after an equilibration time of 3 months at different KOH concentrations.

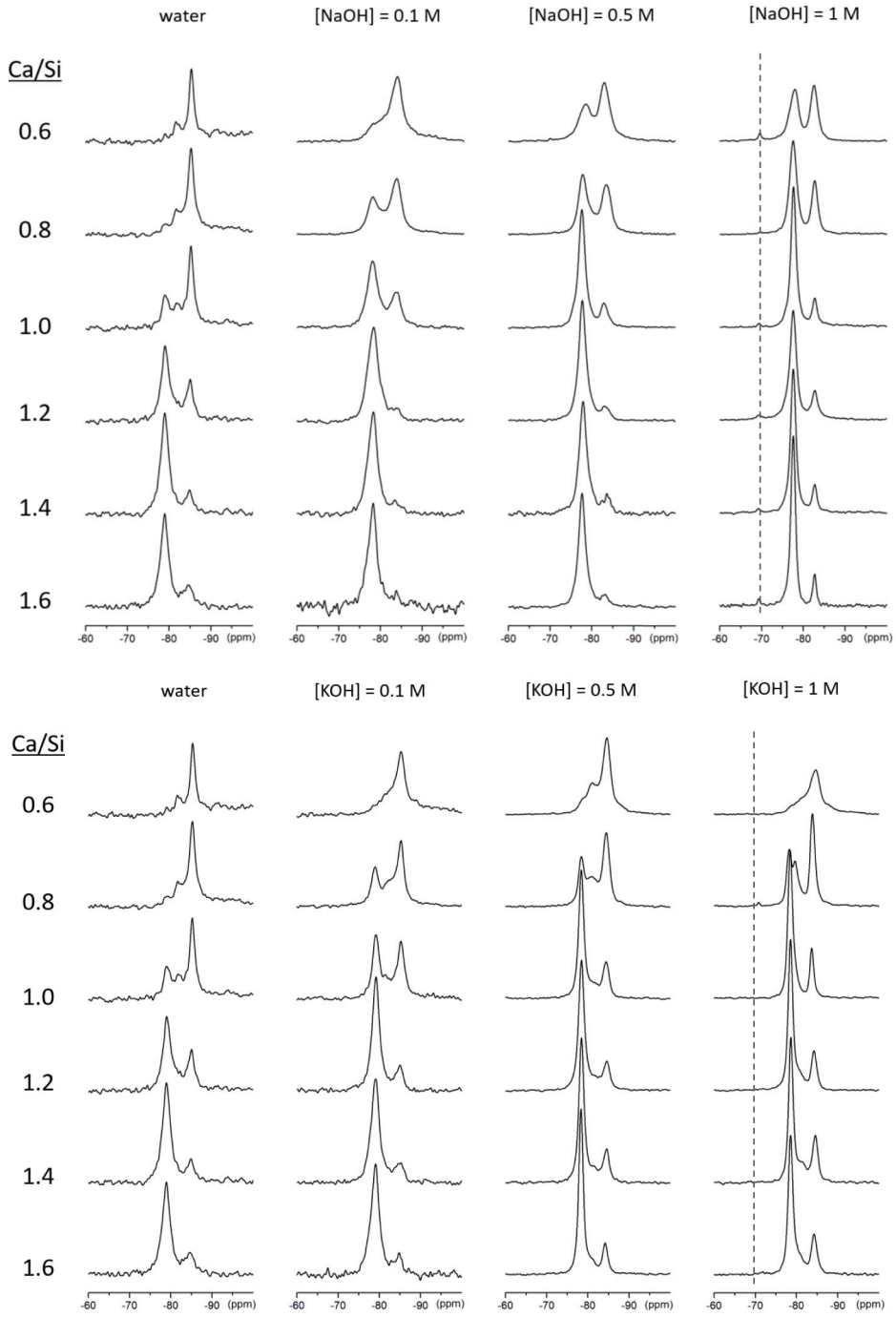

Fig. A4. NMR spectra of C-(N,K-)S-H synthesized in different NaOH and concentrations after an equilibration time of 3 months. The dashed line located at ~ − 70 ppm indicates the Q^0 signal.

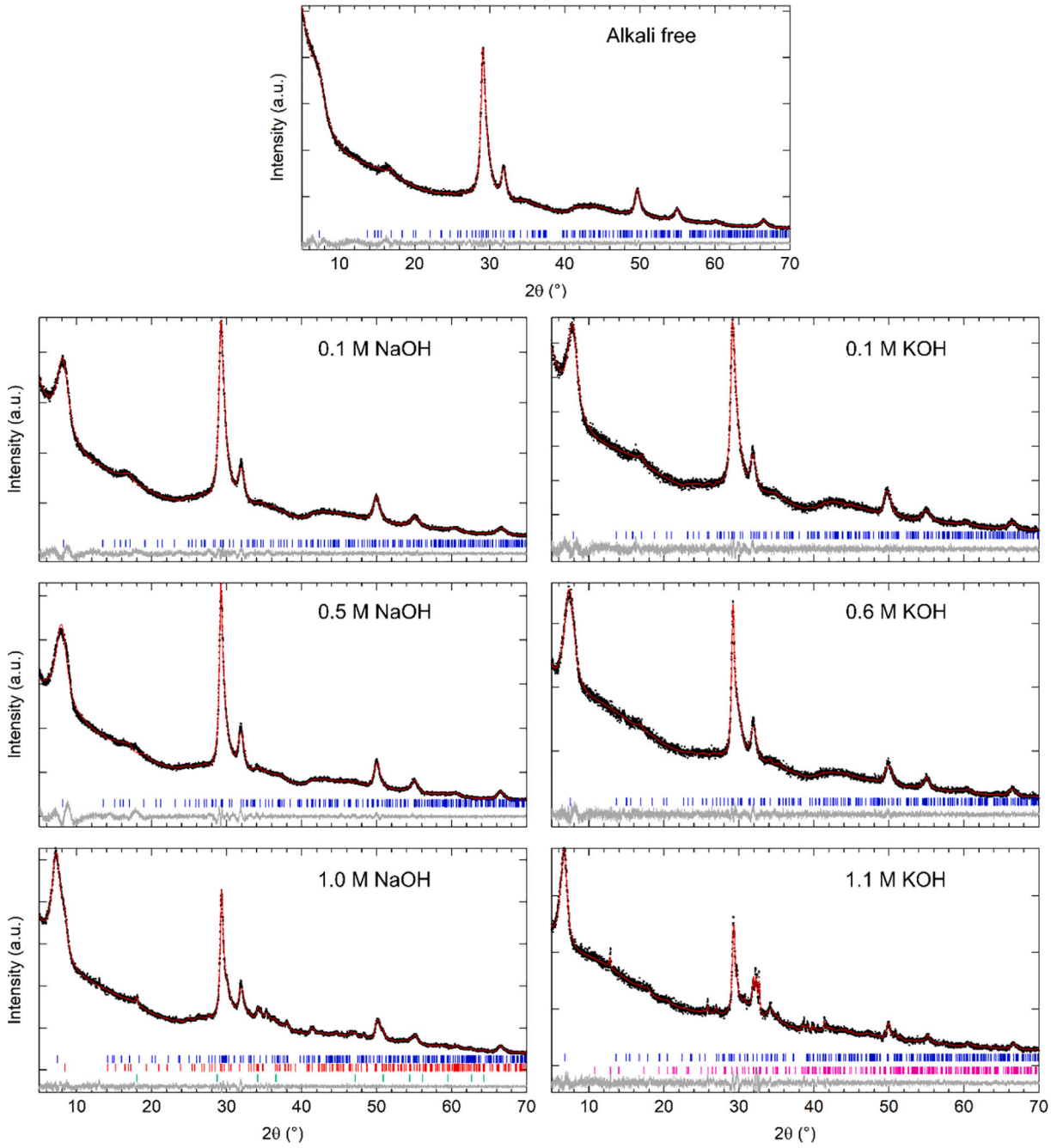

Fig. A5. Pawley fits of the tobermorite 11 Å and 14 Å (for 1.0 M KOH) model to the C-(N,K-)S-H powder patterns with $Ca/Si_{target} = 1.0$. Experimental data are shown as black points, red line as the fit, grey line the data-fit curve, and the blue hkl tick marks for tobermorite reflections. In the case of 1.1 M KOH, an additional impurity phase of $K_2CO_3{\cdot}1.5H_2O$ (PDF# 00-011-0655) was present, which was Rietveld refined with the pink hkl tick marks indicating the reflections. For the 1.0 M NaOH synthesis condition, two reflections are visible for the first diffraction peak, therefore two tobermorite 11 Å models were used to fit the data (shown by the blue and red hkl tick marks). These have different c-axis and crystallite size along the c-direction parameters, but all other parameters are kept equal between the two phases. In addition, the portlandite impurity phase was present and was Rietveld refined with the green hkl tick marks indicating the reflection positions.

References

[1] The Global Cement Report, 13th ed., Tradeship Publications Ltd, Dorking, 2019.
[2] I.G. Richardson, Nature of C-S-H in hardened cements, Cem. Concr. Res. 29 (1999) 1131–1147.
[3] A.J. Allen, J.J. Thomas, H.M. Jennings, Composition and density of nanoscale calcium-silicate-hydrate in cement, Nat. Mater. 6 (2007) 311–316.
[4] L.B. Skinner, S.R. Chae, C.J. Benmore, H.R. Wenk, P.J.M. Monteiro, Nanostructure of calcium silicate hydrates in cements, Phys. Rev. Lett. 104 (2010), 195502.
[5] B. Lothenbach, A. Nonat, Calcium silicate hydrates: solid and liquid phase composition, Cem. Concr. Res. 78 (2015) 57–70.
[6] C.S. Walker, S. Sutou, C. Oda, M. Mihara, A. Honda, Calcium silicate hydrate (C-S-H) gel solubility data and a discrete solid phase model at 25 °C based on two binary non-ideal solid solutions, Cem. Concr. Res. 79 (2016) 1–30.
[7] J. Li, G. Geng, R. Myers, Y.S. Yu, D. Shapiro, C. Carraro, R. Maboudian, P.J. M. Monteiro, The chemistry and structure of calcium (alumino) silicate hydrate: a study by XANES, ptychographic imaging, and wide- and small-angle scattering, Cem. Concr. Res. 115 (2019) 367–378.
[8] G. Geng, R.J. Myers, M.J.A. Qomi, et al., Densification of the interlayer spacing governs the nanomechanical properties of calcium-silicate-hydrate, Sci. Rep. 7 (2017), 10986.

[9] G. Geng, R. Nikolayevich, J. Li, M. Javad, A. Qomi, J. Yan, H. Wenk, P.J. M. Monteiro, Preferred orientation of calcium aluminosilicate hydrate induced by confined compression, Cem. Concr. Res. 113 (2018) 186–196.
[10] J. Li, W. Zhang, K. Garbev, P.J.M. Monteiro, Coordination environment of Si in calcium silicate hydrates, silicate minerals, and blast furnace slags: a XANES database, Cem. Concr. Res. 143 (2021), 106376.
[11] J.J. Chen, J.J. Thomas, H.F.W. Taylor, H.M. Jennings, Solubility and structure of calcium silicate hydrate 34 (2004) 1499–1519.
[12] X. Cong, R.J. Kirkpatrick, R.James Kirkpatrick, 29Si MAS NMR study of the structure of calcium silicate hydrate, Adv. Cem. Based Mater. 3 (1996) 144–156.
[13] I.G. Richardson, The calcium silicate hydrates, Cem. Concr. Res. 38 (2008) 137–158.
[14] I.G. Richardson, J. Skibsted, L. Black, R.J. Kirkpatrick, Characterisation of cement hydrate phases by TEM, NMR and raman spectroscopy, Adv. Cem. Res. 22 (2010) 233–248.
[15] I.G. Richardson, Model structures for C-(A)-S-H(I), Acta Crystallogr. Sect. B Struct. Sci. Cryst. Eng. Mater. 70 (2014) 903–923.
[16] J. Haas, A. Nonat, From C-S-H to C-A-S-H: experimental study and thermodynamic modelling, Cem. Concr. Res. 68 (2015) 124–138.
[17] T.F. Sevelsted, J. Skibsted, Carbonation of C-S-H and C-A-S-H samples studied by 13C, 27Al and 29Si MAS NMR spectroscopy, Cem. Concr. Res. 71 (2015) 56–65.
[18] E. L'Hôpital, B. Lothenbach, D.A. Kulik, K. Scrivener, Influence of calcium to silica ratio on aluminium uptake in calcium silicate hydrate, Cem. Concr. Res. 85 (2016) 111–121.
[19] E. L'Hôpital, B. Lothenbach, G. Le Saout, D. Kulik, K. Scrivener, Incorporation of aluminium in calcium-silicate-hydrates, Cem. Concr. Res. 75 (2015) 91–103.
[20] A. Gruskovnjak, B. Lothenbach, L. Holzer, R. Figi, F. Winnefeld, Hydration of alkali-activated slag: comparison with ordinary Portland cement, Advances Cem. Res. 18 (2006) 119–128.
[21] R.J. Myers, S.A. Bernal, J.L. Provis, A thermodynamic model for C-(N-)A-S-H gel: CNASH_ss. Derivation and validation, Cem. Concr. Res. 66 (2014) 27–47.
[22] Z. Shi, B. Lothenbach, The combined effect of potassium, sodium and calcium on the formation of alkali-silica reaction products, Cem. Concr. Res. 127 (2020), 105914.
[23] J. Lindgård, Ö. Andiç-Çakir, I. Fernandes, T.F. Rønning, M.D.A. Thomas, Alkali-silica reactions (ASR): literature review on parameters influencing laboratory performance testing, Cem. Concr. Res. 42 (2012) 223–243.
[24] T.T.H. Bach, E. Chabas, I. Pochard, C. Cau Dit Coumes, J. Haas, F. Frizon, A. Nonat, Retention of alkali ions by hydrated low-pH cements: mechanism and Na+/K+ selectivity, Cem. Concr. Res. 51 (2013) 14–21.
[25] S. Barzgar, B. Lothenbach, M. Tarik, A. Di Giacomo, C. Ludwig, The effect of sodium hydroxide on Al uptake by calcium silicate hydrates (C-S-H), J. Colloid Interface Sci. 572 (2020) 246–256.
[26] E. L'Hôpital, B. Lothenbach, K. Scrivener, D.A.A. Kulik, Alkali uptake in calcium alumina silicate hydrate (C-A-S-H), Cem. Concr. Res. 85 (2016) 122–136.
[27] R.J. Myers, E.L. Hôpital, L. Provis, B. Lothenbach, Composition-solubility-structure relationships in calcium (alkali) aluminosilicate hydrate (C-(N, K-)A-S-H), Dalt. Trans. 44 (2015) 13530–13544.
[28] C. Labbez, I. Pochard, B. Jönsson, A. Nonat, C-S-H/solution interface: Experimental and Monte Carlo studies, Cem. Concr. Res. 41 (2011) 161–168.
[29] J. Skibsted, M.D. Andersen, The effect of alkali ions on the incorporation of aluminum in the calcium silicate hydrate (C-S-H) phase resulting from Portland cement hydration studied by 29Si MAS NMR, J. Am. Ceram. Soc. 96 (2013) 651–656.
[30] E. Bernard, Y. Yan, B. Lothenbach, Effective cation exchange capacity of calcium silicate hydrates (C-S-H), Cem. Concr. Res. 143 (2021), 106393.
[31] C. Labbez, A. Nonat, I. Pochard, B. Jönsson, Experimental and theoretical evidence of overcharging of calcium silicate hydrate, J. Colloid Interface Sci. 309 (2007) 303–307.
[32] S.V. Churakov, C. Labbez, L. Pegado, M. Sulpizi, Intrinsic acidity of surface sites in calcium silicate hydrates and its implication to their electrokinetic properties, J. Phys. Chem. C 118 (2014) 11752–11762.
[33] N. Krattiger, B. Lothenbach, S.V. Churakov, Sorption and electrokinetic properties of ASR product and C-S-H: a comparative modelling study, Cem. Concr. Res. 146 (2021), 106491.
[34] H. Stade, On the reaction of C-S-H(di, poly) with alkali hydroxides, Cem. Concr. Res. 19 (1989) 802–810.
[35] G. Zhu, H. Li, X. Wang, S. Li, X. Hou, W. Wu, Q. Tang, G. Scherer, Synthesis of calcium silicate hydrate in highly alkaline system, J. Am. Ceram. Soc. 99 (2016) 2778–2785.
[36] N. Garg, V.O. Özçelik, J. Skibsted, C.E. White, Nanoscale ordering and depolymerization of calcium silicate hydrates in the presence of alkalis, J. Phys. Chem. C 123 (2019) 24873–24883.
[37] S. Hong, F.P. Glasser, Alkali binding in cement pastes: part I. The C-S-H phase, Cem. Concr. Res. 29 (1999) 1893–1903.
[38] J. Tits, E. Wieland, C.J. Müller, C. Landesman, M.H. Bradbury, Strontium binding by calcium silicate hydrates, J. Colloid Interface Sci. 300 (2006) 78–87.
[39] M. Tsuji, S. Komarneni, Alkali metal ion exchange selectivity of Al-substituted tobermorite, J. Mater. Res. 4 (1989) 698–703.
[40] A. Leemann, L. Lörtscher, L. Bernard, G. Le, B. Lothenbach, R.M. Espinosa-marzal, Mitigation of ASR by the use of LiNO 3 — characterization of the reaction products, Cem. Concr. Res. 59 (2014) 73–86.
[41] T. H F W, A method for predicting alkali ion concentrations in cement pore solutions (1987), Adv. Cem. Res. 1 (1987) 5–17.
[42] H. Viallis-Terrisse, A. Nonat, J.C. Petit, Zeta-potential study of calcium silicate hydrates interacting with alkaline cations, J. Colloid Interface Sci. 244 (2001) 58–65.
[43] K. Garbev, B. Gasharova, P. Stemmermann, A modular concept of crystal structure applied to the thermal transformation of α-C2 SH, J. Am. Ceram. Soc. 97 (2014) 2286–2297.
[44] I. García Lodeiro, A. Fernández-Jimenez, A. Palomo, D.E. Macphee, Effect on fresh C-S-H gels of the simultaneous addition of alkali and aluminium, Cem. Concr. Res. 40 (2010) 27–32.
[45] E. Kapeluszna, Ł. Kotwica, A. Różycka, Ł. Gołek, Incorporation of Al in C-A-S-H gels with various Ca/Si and Al/Si ratio: Microstructural and structural characteristics with DTA/TG, XRD, FTIR and TEM analysis, Constr. Build. Mater. 155 (2017) 643–653.
[46] P. Yu, R.J. Kirkpatrick, B. Poe, P.F. McMillan, X.D. Cong, Structure of calcium silicate hydrate (C–S–H): near-, mid-, and far-infrared spectroscopy, J. Am. Ceram. Soc. 82 (3) (1999) 742–748.
[47] N.V. Chukanov, Infrared spectra of mineral species, Springer, 2014.
[48] D.A. Kulik, G.D. Miron, B. Lothenbach, A structurally-consistent CASH+ sublattice solid solution model for fully hydrated C-S-H phases: thermodynamic basis, methods, and Ca-Si-H2O core sub-model, Cem. Concr. Res. 151 (2022), 106585.
[49] G.D. Miron, D.A. Kulik, Y. Yan, J. Tits, B. Lothenbach, Extensions of CASH+ thermodynamic solid solution model for the uptake of alkali metals and alkaline earth metals in C-S-H, Cem. Concr. Res. (2022) in review.
[50] B. Traynor, H. Uvegi, E. Olivetti, B. Lothenbach, R.J. Myers, Methodology for pH measurement in high alkali cementitious systems, Cem. Concr. Res. 135 (2020), 106122.
[51] B. Lothenbach, P. Durdzinski, K.De Weerdt, Thermogravimetric analysis, in: K. L. Scrivener, R. Snellings, B. Lothenbach (Eds.), A Practical Guide to Microstructural Analysis of Cementitious Materials, CRC Press, Oxford, UK, 2016, pp. 177–212.
[52] S.T. Merlino, E.L. Bonaccorsi, T.H. Armbruster, The real structure of tobermorite 11Å : normal and anomalous forms, OD character and polytypic modifications, Eur. J. Mineral. 13 (2001) 577–590.
[53] A.A. Coelho, TOPAS and TOPAS-academic: an optimization program integrating computer algebra and crystallographic objects written in C++: an, J. Appl. Crystallogr. 51 (2018) 210–218.
[54] E. Bonaccorsi, S. Merlino, A.R. Kampf, The crystal structure of tobermorite 14 Å (plombierite), a C-S-H phase, J. Am. Ceram. Soc. 88 (2005) 505–512.
[55] D. Ectors, F. Goetz-Neunhoeffer, J. Neubauer, A generalized geometric approach to anisotropic peak broadening due to domain morphology, J. Appl. Crystallogr. 48 (2015) 189–194.
[56] J. Skibsted, J. Hjorth, H.J. Jakobsen, Correlation between 29Si NMR chemical shifts and mean SiO bond lengths for calcium silicates, Chem. Phys. Lett. 172 (1990) 279–283.
[57] D. Massiot, F. Fayon, M. Capron, I. King, L. Calv, B. Alonso, J. Durand, B. Bujoli, Z. Gan, G. Hoatson, Modelling one- and two-dimensional solid-state NMR, Magn. Reson. Chem. 40 (2002) 70–76.
[58] S.-Y. Yang, Y. Yan, B. Lothenbach, J. Skibsted, Sodium and tetrahedral aluminium in cementitious calcium-aluminate-silicate hydrate phases (C-A-S-H), J. Phys. Chem. C. (2021) in review.
[59] T. Wagner, D.A. Kulik, F.F. Hingerl, S.V. Dmytrievava, GEM-Selektor geochemical modeling package: TSolMod library and data interface for multicomponent phase models, Can. Mineral. 50 (2012) 1173–1195.
[60] T. Thoenen, W. Hummel, U. Berner, E. Curti, The PSI/Nagra Chemical Thermodynamic Database 12/07, 5232 Villigen PSI, 2014.
[61] B. Lothenbach, D.A. Kulik, T. Matschei, M. Balonis, L. Baquerizo, B. Dilnesa, G. D. Miron, R.J. Myers, Cemdata18: a chemical thermodynamic database for hydrated Portland cements and alkali-activated materials, Cem. Concr. Res. 115 (2019) 472–506.
[62] S. Masoumi, S. Zare, H. Valipour, M.J.Abdolhosseini Qomi, Effective interactions between calcium-silicate-hydrate nanolayers, J. Phys. Chem. C. 123 (2019) 4755–4766.
[63] S. Grangeon, F. Claret, Y. Linard, C. Chiaberge, X-ray diffraction: a powerful tool to probe and understand the structure of nanocrystalline calcium silicate hydrates, Acta Crystallogr. Sect. B Struct. Sci. Cryst. Eng. Mater. 69 (2013) 465–473.
[64] V. Stubičan, R. Roy, Infrared spectra of layer-structure silicates, J. Am. Ceram. Soc. 44 (1961) 625–627.
[65] A. Vidmer, G. Sclauzero, A. Pasquarello, Infrared spectra of jennite and tobermorite from first-principles, Cem. Concr. Res. 60 (2014) 11–23.
[66] I.F. Sáez Del Bosque, S. Martínez-Ramírez, M.T. Blanco-Varela, FTIR study of the effect of temperature and nanosilica on the nano structure of C-S-H gel formed by hydrating tricalcium silicate, Constr. Build. Mater. 52 (2014) 314–323.
[67] I. García Lodeiro, D.E. Macphee, A. Palomo, A. Fernández-Jiménez, Effect of alkalis on fresh C-S-H gels. FTIR analysis, Cem. Concr. Res. 39 (2009) 147–153.
[68] J. Higl, D. Hinder, C. Rathgeber, B. Ramming, M. Lindén, Detailed in situ ATR-FTIR spectroscopy study of the early stages of C-S-H formation during hydration of monoclinic C3S, Cem. Concr. Res. 142 (2021), 106367.
[69] R.J. Kirkpartick, J.L. Yarger, P.F. McMillan, P. Yu, X. Cong, Raman spectroscopy of C-S-H, tobermorite, and jennite, Adv. Cem. Based Mater. 5 (1997) 93–99.
[70] K. Garbev, P. Stemmermann, L. Black, C. Breen, J. Yarwood, B. Gasharova, Structural features of C-S-H(I) and its carbonation in air-a raman spectroscopic study. Part I: fresh phases, J. Am. Ceram. Soc. 90 (2007) 900–907.
[71] G. Renaudin, J. Russias, F. Leroux, C. Cau-dit-Coumes, F. Frizon, Structural characterization of C-S-H and C-A-S-H samples-part II: local environment investigated by spectroscopic analyses, J. Solid State Chem. 182 (2009) 3320–3329.

[72] Z. Shi, G. Geng, A. Leemann, B. Lothenbach, Synthesis, characterization, and water uptake property of alkali-silica reaction products, Cem. Concr. Res. 121 (2019) 58–71.
[73] S. Ortaboy, J. Li, G. Geng, R.J. Myers, P.J.M.M. Monteiro, R. Maboudian, C. Carraro, Effects of CO2 and temperature on the structure and chemistry of C-(A-)S-H investigated by raman spectroscopy, RSC Adv. 7 (2017) 48925–48933.
[74] R. Dupuis, J.S. Dolado, J. Surga, A. Ayuela, Doping as a way to protect silicate chains in calcium silicate hydrates, ACS Sustain. Chem. Eng. 6 (2018) 15015–15021.
[75] C. Famy, K.L. Scrivener, A.K. Crumbie, What causes differences of C-S-H gel grey levels in backscattered electron images? Cem. Concr. Res. 32 (2002) 1465–1471.
[76] S.V. Churakov, C. Labbez, Thermodynamics and molecular mechanism of Al incorporation in calcium silicate hydrates, J. Phys. Chem. C 121 (2017) 4412–4419.
[77] S.-Y. Hong, F.P. Glasser, Alkali sorption by C-S-H and C-A-S-H gels: part II. Role of alumina, Cem. Concr. Res. 32 (2002) 1101–1111.
[78] R.J. Myers, E. L'Hôpital, J.L. Provis, B. Lothenbach, Effect of temperature and aluminium on calcium (alumino)silicate hydrate chemistry under equilibrium conditions, Cem. Concr. Res. 68 (2015) 83–93.
[79] C. Roosz, P. Vieillard, P. Blanc, S. Gaboreau, H. Gailhanou, D. Braithwaite, V. Montouillout, R. Denoyel, P. Henocq, B. Madé, Thermodynamic properties of C-S-H, C-A-S-H and M-S-H phases: results from direct measurements and predictive modelling, Appl. Geochemistry. 92 (2018) 140–156.
[80] A.C.A. Muller, K.L. Scrivener, A.M. Gajewicz, P.J. McDonald, Use of bench-top NMR to measure the density, composition and desorption isotherm of C-S-H in cement paste, Microporous Mesoporous Mater. 178 (2013) 99–103.
[81] G. Renaudin, J. Russias, F. Leroux, F. Frizon, C. Cau-dit-Coumes, Structural characterization of C-S-H and C-A-S-H samples-part I: long-range order investigated by rietveld analyses, J. Solid State Chem. 182 (2009) 3312–3319.
[82] G. Geng, R.J. Myers, J. Li, R. Maboudian, C. Carraro, D.A. Shapiro, P.J. Monteiro, Aluminum-induced dreierketten chain cross-links increase the mechanical properties of nanocrystalline calcium aluminosilicate hydrate, Sci. Rep. 7 (2017), 44032.
[83] Y.L. Yaphary, D. Lau, F. Sanchez, C.S. Poon, Effects of sodium/calcium cation exchange on the mechanical properties of calcium silicate hydrate (C-S-H), Constr. Build. Mater. 243 (2020), 118283.
[84] I. Lognot, I. Klur, A. Nonae, NMR and infrared spectroscopies of C-S-H and AI-substituted C-S-H synthesised in alkaline solutions, in: Nucl. Magn. Reson. Spectrosc. Cem. -Based Mater, 1998, pp. 189–196.
[85] P. Nieto, H. Zanni, Polymerization of alkaline-calcium-silicate hydrates obtained by interaction between alkali-silica solutions and calcium compounds. A 29Si nuclear magnetic resonance study, J. Mater. Sci. 32 (1997) 3419–3425.